

1 **Investigation of Rare Earth Element Binding to a Surface-Bound Affinity Peptide Derived**  
2 **from EF-Hand Loop I of Lanmodulin**

3 Geeta Verma<sup>†,1</sup>, Jacob Hostert<sup>†,1</sup>, Alex A. Summerville<sup>1</sup>, Alicia S. Robang<sup>2</sup>, Ricardo Garcia  
4 Carcamo<sup>3</sup>, Anant K. Paravastu<sup>2,4</sup>, Rachel B. Getman<sup>3</sup>, Christine Duval<sup>1</sup> and Julie Renner<sup>\*,1</sup>

5 <sup>1</sup>Department of Chemical and Biomolecular Engineering, Case Western Reserve University,  
6 Cleveland, Ohio 44106

7 <sup>2</sup>School of Chemical and Biomolecular Engineering, Georgia Institute of Technology, Atlanta,  
8 Georgia 30332

9 <sup>3</sup>Departemnt of Chemical and Biomolecular Engineering, Ohio State University, Columbus, OH  
10 43210

11 <sup>4</sup>Parker H. Petit Institute for Bioengineering and Biosciences, Georgia Institute of Technology,  
12 315 Ferst Drive, Atlanta, 30332, GA, USA

13 <sup>†</sup> Co-first author

14 <sup>\*</sup>Corresponding Author ([jxr484@case.edu](mailto:jxr484@case.edu))

15 **Abstract**

16 Bioinspired strategies have been given extensive attention for the recovery of rare earth elements  
17 (REEs) from waste streams because of their high selectivity, regeneration potential, and  
18 sustainability, as well as low cost. Lanmodulin protein is an emerging biotechnology that is highly  
19 selective for REE binding. Mimicking lanmodulin with shorter peptides is advantageous because  
20 they are simpler and potentially easier to manipulate and optimize. Lanmodulin-derived peptides  
21 have been found to bind REEs, but their properties have not been explored when immobilized on  
22 the solid substrates, which is required for many advanced separation technologies. Here, two  
23 peptides, LanM1 and scrambled LanM1 are designed from the EF-hand loop 1 of lanmodulin and  
24 investigated for their binding affinity towards different REEs when surface-bound. First, the ability  
25 for LanM1 to bind REEs was confirmed and characterized in solution, using circular dichroism  
26 (CD), nuclear magnetic resonance (NMR), and molecular dynamics (MD) simulations for Ce (III)

27 ions. Isothermal titration calorimetry (ITC) was used to further analyze the binding of the LanM1  
28 to Ce (III), Nd (III), Eu (III) and Y(III) ions and in low pH conditions. The performance of the  
29 immobilized peptides on a model gold surface was examined using quartz crystal microbalance  
30 with dissipation (QCM-D). The studies show LanM1 peptide has a stronger REE binding affinity  
31 than scrambled LanM1 when in solution and when immobilized on a gold surface. QCM-D data  
32 were fit to the Langmuir adsorption model to estimate the surface-bound dissociation constant ( $K_d$ )  
33 of LanM1 with Ce (III) and Nd (III). The results indicate LanM1 peptides maintain high affinity  
34 for REEs when immobilized, and surface-bound LanM1 has no affinity for potential competitor  
35 calcium and copper ions. The utility of surface-bound LanM1 peptides was further demonstrated  
36 by immobilizing them to gold nanoparticles (GNPs) and capturing REEs from solution in  
37 experiments utilizing an arsenazo-III based colorimetric dye-displacement assay and UV-vis  
38 spectrophotometry. The saturated adsorption capacity of GNPs was estimated to be around 3.5  
39  $\mu\text{mol REE/g}$  for Ce (III), Nd (III), Eu (III) and Y(III) ions, with no binding of non-REE Ca (II)  
40 ions observed.

#### 41 **Keywords**

42 Rare-earth elements (REEs), biosorption, gold nanoparticles, affinity peptides, lanmodulin,  
43 molecular dynamics.

#### 44 **1 Introduction**

45 Rare-earth elements (REEs) are essential in several emerging technologies such as wind turbines,  
46 electric vehicles, computer memory, autocatalytic converters, magnetic resonance imaging, and  
47 smartphones.<sup>1</sup> Owing to the high cost and limited availability, the recovery of these elements from  
48 the industrial waste streams is an attractive option for a green and circular economy.<sup>2</sup> There is an  
49 urgent need to identify efficient separation methods that recycle REEs from the waste streams and  
50 provide a steady, domestic source of these elements. Various techniques have been applied to  
51 recover REEs from the waste streams such as solvent extraction,<sup>3</sup> filtration,<sup>4</sup> ion exchange,<sup>5</sup>  
52 chemical precipitation,<sup>6</sup> adsorption,<sup>7</sup> and electrochemical processes.<sup>8</sup> Commercially, solvent

53 extraction is used to separate REEs from concentrated aqueous waste streams but the solvent  
54 requirements are high in this method.<sup>9</sup> Membrane filtration techniques do well under low  
55 concentration and high volume throughput conditions but the limiting factor is the selectivity of  
56 commercial membranes for trivalent ions over divalent ions.<sup>10</sup> Overall, some of the constraints of  
57 these methods include high chemical consumption, high operational cost and the need to treat the  
58 generated waste.<sup>11</sup> To overcome these challenges, innovative developments utilizing several  
59 emerging technologies such as nanomaterials, bioleaching, biosorption, acidolysis,  
60 biomineralization, cryo-milling, and the use of supercritical CO<sub>2</sub><sup>12</sup> are under investigation. Among  
61 these, there are several advantages of bio-combined (biosorption) recycling strategies as they show  
62 higher selectivity, use fewer toxic chemicals, have high regeneration potential, demonstrate fast  
63 kinetics, and are cost-efficient.<sup>13</sup> However, the design of a bio-based approach with selective  
64 adsorption of REEs requires deep acquaintance with the support materials and the ligand of choice  
65 such as peptides that can be grafted on the desired surface for selective separation of REEs.  
66 Peptides are desirable as they are short chains of amino acids (less than 50) and are highly tunable  
67 ligands that are selective for ions.<sup>14</sup> Many researchers have attempted to identify or design peptides  
68 with the ability to selectively bind to lanthanides.<sup>13, 15, 16</sup> For example, Hatanaka *et al.*<sup>15</sup> studied a  
69 linear peptide lanthanide binding tag (LBT3) and by combining experimental and computational  
70 techniques provided a deep insight into the mechanism underlying the specificity of the peptide  
71 toward lanthanides in aqueous media. Through isothermal titration calorimetry (ITC) experiments,  
72 they found that the thermodynamic properties of ion complexation strongly vary with lanthanide  
73 ion size and molecular dynamics (MD) simulations revealed that the high binding affinity is  
74 achieved through complete ion dehydration. In another investigation, Xu *et al.*<sup>16</sup> derived a peptide  
75 sequence from the EF-hand loop I of calmodulin and experimentally showed that the peptide has

76 the same affinity for cerium (III) ions when tethered to a gold surface (surface-bound) as it does  
77 in solution (unbound).<sup>16, 17</sup>

78 The recent discovery of the lanmodulin protein, which has high selectivity for REEs over non-  
79 REEs,<sup>18</sup> opens new possibilities for utilizing lanmodulin-derived peptides for REE recovery.

80 Lanmodulin has four metal-binding EF-hand motifs that undergo a large conformational change  
81 in response to REE binding (from a largely disordered state to a more ordered state) and has higher  
82 affinity over calmodulin.<sup>19</sup> As a result, several lanmodulin-ion complexation studies have been

83 conducted to understand its structure as well as its REE binding affinity and selectivity.<sup>19-24</sup> In a

84 recent investigation of the four EF-hand loop peptides derived from lanmodulin, Gutenthaler *et*  
85 *al.*<sup>24</sup> examined their affinity for two REEs (Eu(III), Tb(III)) and one non-REE (Ca(II)) in solution

86 and used molecular dynamics simulations to further support their experimental observations.

87 While studies of the shorter peptides are limited, more work has been done to tether the full-length  
88 lanmodulin protein to various supports to perform separation. Kwon and co-workers<sup>21</sup> used elastin-

89 like polypeptide (ELP) fused with truncated lanmodulin protein to form REEs-sensitive and  
90 thermo-responsive genetically encoded ELP, called "RELP". They studied several REEs ((Tb (III),

91 La (III), Ce (III) and Y(III)) and non-REEs (Zn (II) and Cu (II)) in bulk with the help of  
92 calorimetric techniques. Among limited solid surface-bound studies, Dong *et al.*, immobilized

93 lanmodulin protein on agarose microbeads through thiol-maleimide click chemistry and  
94 investigated the selectivity between REE pairs (Nd (III)/Dy (III), and Y (III)/Nd (III)) and grouped

95 separation between heavy REEs (Tb(III)-Lu(III)+Y(III)) over light REEs (La(III)-Gd (III)) on a  
96 resin-packed column.<sup>22</sup> Ye *et al.*<sup>23</sup> immobilized lanmodulin protein on the surface of magnetic

97 nanoparticles (MNPs) through SpyTag-SpyCatcher (Spy) chemistry and studied the binding of  
98 several REEs and non-REEs. Xiaoman *et al.* engineered a bio-adsorbent in which lanmodulin was

99 displayed on the cell surface of the fungus *Yarrowia lipolytica* and the binding capacity for  
100 different REEs and non-REEs was characterized.<sup>20</sup> Although there are a few studies done on  
101 surface-bound lanmodulin protein, no such investigation has been done on lanmodulin-derived  
102 peptide for REE binding.

103 In this work, two novel peptides, LanM1, and scrambled LanM1 are derived from the EF-hand  
104 loop 1 of lanmodulin and are investigated against four REEs (Ce (III), Nd (III), Eu (III) and Y(III)),  
105 and two competing non-REEs (Ca (II) and Cu (II)) in surface-bound and unbound conditions.  
106 Cerium is selected as it is an important material in a wide range of applications such as oxygen  
107 sensing, industrial catalysis, fuel cells, low-temperature water-gas shift reactions, and  
108 electrochromic thin-film application.<sup>25, 26</sup> Neodymium is used mainly in magnets, catalysts, and  
109 lasers.<sup>27</sup> Europium has applications in control rods for nuclear reactors, fluorescent bulbs and  
110 optoelectronics<sup>1, 28</sup>. The common use of yttrium is in lasers, fluorescent lamps, and lighting.<sup>27, 29</sup>  
111 We performed circular dichroism (CD) analysis and nuclear magnetic resonance (NMR) to  
112 confirm that the LanM1 peptide sequence modified for surface immobilization binds REEs.  
113 Isothermal calorimetry (ITC) experiments were performed to determine the thermodynamic  
114 parameters ( $K_D$ ,  $\Delta H$ ,  $\Delta S$ , and  $\Delta G$ ) of the interaction between the peptides and the ions in solutions.  
115 QCM-D was conducted to show that surface-bound peptides derived from lanmodulin can bind  
116 REEs and characterize the surface-bound affinity using the Langmuir adsorption model to estimate  
117 equilibrium binding constants. Molecular dynamics simulations were performed to gain molecular  
118 insight and to complement the experimental results. Finally, to demonstrate the utility of the  
119 surface-bound peptide as a material, the maximum REE adsorption capacity of LanM1  
120 immobilized on gold nanoparticles was determined in a proof-of-concept experiment. Overall, this  
121 study characterizes the properties of surface-bound LanM1 peptide for the first time, and

122 demonstrates its potential utility in REE separation for further optimization and exploration in the  
123 future.

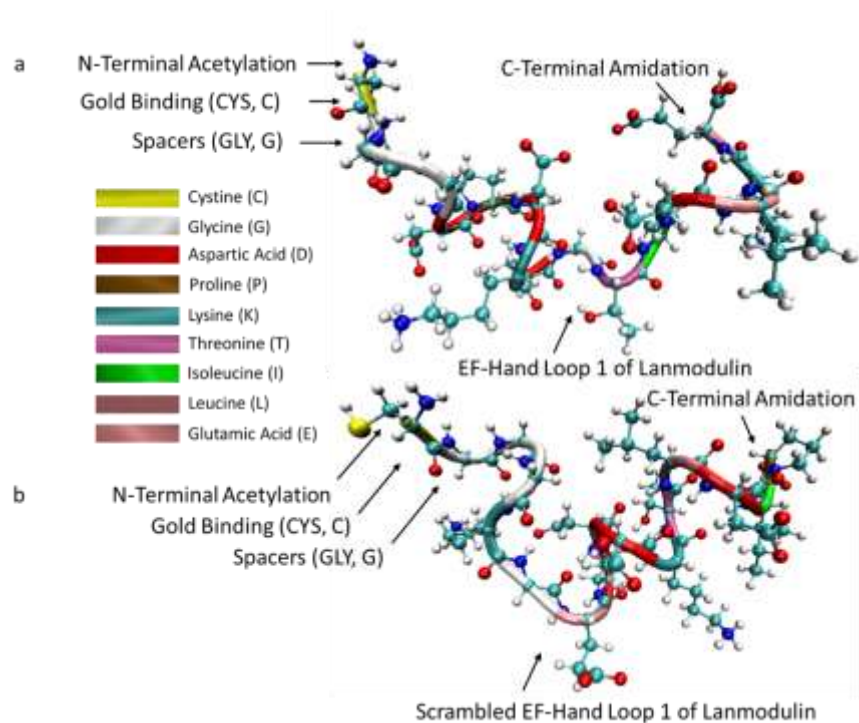
## 124 **Materials and Methods**

### 125 **Materials**

126 The peptide sequences in this study were derived from the EF-hand loop I of lanmodulin and were  
127 ordered from GenScript (<https://www.genscript.com/>) at a purity of >95%. Cerium (III) chloride  
128 heptahydrate ( $\text{CeCl}_3 \cdot 7\text{H}_2\text{O}$ ) 99.9% purity, neodymium nitrate hexahydrate ( $\text{Nd}(\text{NO}_3)_3 \cdot 6\text{H}_2\text{O}$ )  
129 99.9% purity, europium (III) chloride hexahydrate ( $\text{EuCl}_3 \cdot 6\text{H}_2\text{O}$ ) 99.9% purity, yttrium (III)  
130 chloride hexahydrate ( $\text{YCl}_3 \cdot 6\text{H}_2\text{O}$ ) 99.9% purity, calcium sulfate dihydrate ( $\text{CaSO}_4 \cdot 2\text{H}_2\text{O}$ ) 99.0 %  
131 purity and copper sulfate pentahydrate ( $\text{CuSO}_4 \cdot 5\text{H}_2\text{O}$ ) 99.9% purity were purchased from Sigma-  
132 Aldrich. Millipore ultrapure water (UPW) was used as a solvent. Nitrogen ( $\text{N}_2$ ) gas (>99%) that  
133 was used in circular dichroism experiments was procured from Airgas. Gold nanoparticles with  
134 size less than 100 nm (powder), 99.9% trace were obtained from Sigma-Aldrich.

### 135 **Peptide Design**

136 The peptide sequences for binding studies were designed from EF-hand loop I of lanmodulin. The  
137 sequence intended for REE binding is called LanM1 ( $\text{Ac-CGGGDPDKDGTIDLKE-NH}_2$ ). It is  
138 the same sequence as the EF hand loop I of lanmodulin with additional three glycine amino acids  
139 as spacers and one cystine residue for binding to the gold surface. A schematic representation of  
140 LanM1 is given in **Figure 1a**. The second sequence, called scrambled LanM1 ( $\text{Ac-}$   
141  $\text{CGGGKGEDDDKTLDIP-NH}_2$ ), has the same amino acids as in EF-hand loop I of lanmodulin  
142 but are randomly arranged with the same three glycine amino acids as spacers and one cystine for  
143 binding to the gold surface (**Figure 1b**). For both peptides, N-terminal acetylation and C-terminal  
144 amidation was done to increase the stability by reducing degradation.



145

146 **Figure 1.** (a) Schematic representations of the energy minimized peptide sequences LanM1 (Ac-  
 147 CGGGDPDKDGTIDLKE-NH<sub>2</sub>) and (b) scrambled LanM1 (Ac-CGGGKGEDDDKTLDIP-NH<sub>2</sub>)  
 148 designed in this study for cerium binding. Different colors in the backbone (tube representation)  
 149 are used to show different amino acids in the sequence. The energy-minimized molecular images  
 150 of the peptides were created using the Visual Molecular Dynamics (VMD) package.<sup>30</sup>

151 **Circular Dichroism (CD)**

152 A circular dichroism (CD) spectrometer (Jasco J-815) was used to examine the conformational  
 153 change of the peptides under the influence of cerium (III) in ultrapure water. The step resolution  
 154 of 0.1 nm, and the scanning speed of 20 nm/min were selected to scan the samples in a quartz  
 155 cuvette with a 0.1 cm path length. The absorbance spectra were generated in the range of 190-260  
 156 nm wavelength. The post processing of the data including baseline correction and smoothing of

157 the spectra was done using the Spectra Analysis processing tool of the Spectra Manager ver. 2.0  
158 program which accompanied the spectrometer.

### 159 **<sup>1</sup>H Nuclear Magnetic Resonance (NMR) Measurements**

160 LanM1 and scrambled LanM1 samples were prepared by dissolving 1 mg of peptide in 0.75 mL  
161 of deuterated water (D<sub>2</sub>O) and then pipetting them into 5 mm Wilmad NMR tubes. Each molar  
162 equivalent of cerium (III) was dissolved in 50 μL D<sub>2</sub>O before being added into NMR sample tubes.  
163 NMR measurements were collected on a 11.75 T magnet (500 MHz, <sup>1</sup>H NMR frequency) in a  
164 Bruker spectrometer. The Bruker default “zgesgp” pulse sequence for water suppression using  
165 excitation sculpting was used to collect <sup>1</sup>H spectra. Signals were averaged over 100 scans.

### 166 **Isothermal Titration Calorimetry (ITC)**

167 Isothermal titration calorimetry (ITC) analysis was performed using MicroCal Auto-ITC<sub>200</sub>. In the  
168 present work, 200 μM REE solutions were titrated in 35 injections of 1 μL each with 300 μL  
169 peptide solution (20 mM) at 30<sup>0</sup>C. The solutions were prepared in ultrapure water and prior to  
170 experiments the solutions were degassed. The first injection point was removed due to  
171 dilution/mixing effect and the baseline was corrected prior to further analysis. The data analysis  
172 was done with Origin 7.0 using the one set of sites fitting model to calculate binding constant (K<sub>d</sub>),  
173 enthalpy (ΔH) and entropy (ΔS).

### 174 **Quartz Crystal Microbalance (QCM)**

175 Quartz crystal microbalance with dissipation (QCM-D, Q-Sense Explorer, operated by Q-Soft  
176 integrated software from Biolin Scientific was used to investigate the mass adsorption of the ions  
177 to surface-bound lanmodulin derived peptides. Frequency shifts and dissipation changes were  
178 monitored simultaneously with time, and all experiments were conducted in aqueous solution.

179 Information about the gold-coated crystal sensors (QSX 301, 5 MHz, Biolin Scientific), module  
180 cleaning, and data analysis can be found in our previous work.<sup>31</sup> In general, QCM-D experiments  
181 were operated in a flow module at 18°C and at a flow rate of 150  $\mu\text{L}/\text{min}$ . Frequency decrease and  
182 increase reflects mass accumulation and removal on the surface respectively, and dissipation  
183 changes show the viscoelastic characteristics of the adsorbed material. After acquiring a stable  
184 baseline with ultrapure water, lanmodulin peptides (**Figure 1**) were introduced at 10  $\mu\text{g}/\text{mL}$  in  
185 ultrapure water and allowed to adsorb to the gold surface for ten to twenty minutes before rinsing  
186 with ultrapure water to remove unbound peptide. Next, ion solutions were introduced to bind to  
187 the peptide for at least ten minutes and then rinsed with ultrapure water to remove loosely bound  
188 ions. The QCM-D instrument is not sensitive enough to detect the REE loading on the peptide due  
189 to extremely small added mass. To improve the sensitivity of detecting REE ion binding, a 1 mM  
190 sodium phosphate solution was then introduced for at least ten minutes before a final rinse with  
191 ultrapure water. The exact mechanism of phosphate interaction with REEs is still unclear. We  
192 speculate co-adsorbed water or precipitation along with the phosphate ions intensifies the  
193 frequency change.<sup>17</sup> This technique was validated with a known calmodulin peptide (**Figure S7**).  
194 The mass loading during the adsorption was estimated using QSense Dfind software.

## 195 **MD Simulations**

196 Molecular dynamics (MD) simulations were carried out using the GROMACS package.<sup>32</sup> First,  
197 the peptide sequences were drawn in ChimeraX,<sup>33</sup> and the coordinates were saved in pdb format.  
198 The coordinate files in pdb format were used to generate the topology and other input files using  
199 GROMACS toolkit. By default, termini are ionized ( $\text{NH}_3^+$  and  $\text{COO}^-$ ), therefore it is important to  
200 cap the N- and C-termini of the peptide to make them uncharged ( $\text{NH}_2$  and  $\text{COOH}$ ). Leaving the  
201 termini charged leads to artificial charge-charge interactions, particularly in small molecules like

202 peptides. The CHARMM all-atom force field was selected to model peptides.<sup>34</sup> Cerium (III) was  
203 modeled as LJ sphere with  $\sigma = 0.306$  nm and  $\epsilon = 0.0676$  kcal/mol<sup>35</sup> with comparable parameters  
204 as other previously developed force fields.<sup>36,37</sup> Water molecules were represented with the TIP3P  
205 model as it is widely used for protein ligand simulation.<sup>38</sup> The geometric mixing rule was used to  
206 obtain the interaction parameters between unlike atoms. The initial configurations were generated  
207 by placing the peptides in the center of a cubic box with side length 5 nm. One cerium ion was  
208 inserted at some random position and the boxes were solvated with explicit water molecules. The  
209 periodic boundary conditions were used in all directions. Prior to simulation, the geometries of the  
210 systems were minimized using the steepest descent algorithm to remove any contact between the  
211 atoms. After geometry minimization, the systems were annealed from 600 K to 300 K in NVT  
212 ensemble for 5 ns. This was done to facilitate ion binding, overcome slow dynamics and any energy  
213 barrier, and possible metastable stages. Finally, three independent 50 ns long simulations were  
214 run in NPT ensemble for the analysis. A time step of 2 fs was used with all bonds involving  
215 hydrogen atoms constrained by the LINCS algorithm.<sup>39</sup> The electrostatic interactions were treated  
216 using the fast particle-mesh Ewald (PME) summation method with a cutoff of 1.5 nm and a grid  
217 spacing of 0.1 nm.<sup>40</sup> The temperature was kept constant at 300 K using the velocity-rescale  
218 thermostat with a coupling constant of 0.1 ps.<sup>41</sup> In NPT ensemble, 1 bar pressure was maintained  
219 used the Parrinello-Rahman pressure coupling with a coupling constant of 2.0 ps.<sup>42</sup> The trajectories  
220 obtained from the simulations were visualized in the VMD package and coordination of oxygen  
221 atoms in the binding sites were monitored throughout the simulation.<sup>30</sup> A snapshot of the  
222 equilibrated configuration of the system comprised of the peptide ion complex after 50 ns is shown  
223 in **Figure S1**.

## 224 **Adsorption Experiments on Gold Nanoparticles (GNPs)**

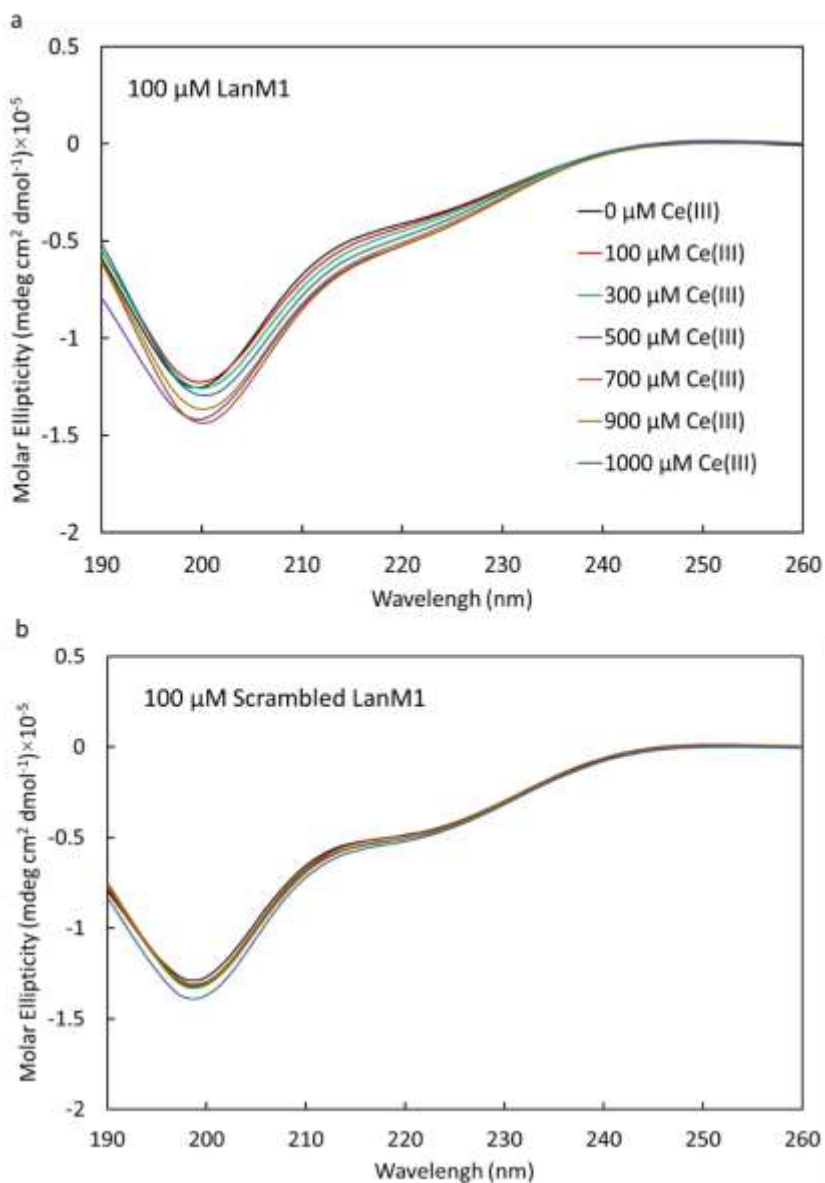
225 A protocol was prepared and used to estimate the adsorption of REEs on LanM1 functionalized  
226 GNPs. In all experiments, roughly 8 to 12 mg of GNP powder was added to 2.0 ml Eppendorf tube  
227 and the exact weight of GNPs was calculated by taking the weight of the tube before and after  
228 adding GNPs. Later, 1 mL LanM1 solution at 60.2  $\mu\text{M}$  concentration was added and the tube was  
229 incubated on the rocker table for 24 hours to saturate the GNPs with the peptide. Once LanM1 was  
230 functionalized on GNPs, the tube was centrifuged, and the supernatant was removed. The LanM1  
231 functionalized GNPs were then rinsed for five times with ultrapure water to assure no unbound  
232 LanM1 was left in the tube. The weight of the tube was measured again to estimate leftover water  
233 as it was not possible to pipette out all water after centrifugation and rinsing. In the following step,  
234 1.5 mL of REE solution at a specific concentration between 20 to 125  $\mu\text{M}$  was added to the tube  
235 and incubated again on a rocker table for another 24 hours. During incubation, the concentration  
236 of GNP in the REE solution was 5-8 mg GNP/mL. After centrifuging the tube, the supernatant was  
237 titrated against arsenazo III reagent and using colorimetric technique, the concentration of the REE  
238 was estimated. Control experiments without GNP were performed to assure that no metal leached  
239 from the tube material into the solution and no REE absorbed on the tube surface. A pictorial  
240 representation of step-by-step procedure used for REE binding on gold nanoparticles (GNPs) is  
241 shown in panel a of Figure 8. The initial and supernatant REE concentrations were used to find the  
242 adsorption capacity of LanM1 functionalized GNPs. The pH of the solution remained between 5.0  
243 to 5.5 throughout the experiment.

## 244 **2 Results and Discussion**

### 245 **Conformational Analysis and Binding Site Investigation**

246 Both the peptides, LanM1 and scrambled LanM1, are newly designed peptides and an initial  
247 binding investigation was needed to identify their ability to bind REE ions in solution. Therefore,

248 the ability to bind to cerium (III) ions was checked using circular dichroism (CD) experiments, as  
249 we have done with other EF-hand peptide sequences previously.<sup>16</sup> Several experiments were  
250 performed by keeping peptide concentration at 100  $\mu$ M and varying cerium (III) ion concentration  
251 within the range of 100 to 1000  $\mu$ M. The effect of ion concentration on the secondary structure of  
252 the peptides was observed and the spectra for LanM1 and scrambled LanM1 are reported in **Figure**  
253 **2a and b**, respectively. In case of LanM1, it was observed that at a wavelength around 222 nm,  
254 there is a decrease in the ellipticity as cerium ion concentration increases. It has been reported that  
255 decreases in the ellipticity at 222 nm are related to an increase in  $\alpha$ -helicity caused by metal  
256 binding.<sup>16, 24</sup> In case of LanM1, a change in the structure of the peptide is confirmed upon REE  
257 binding with shifts at 200 and 222 nm observed. When looking at the spectra of scrambled LanM1,  
258 smaller changes in the ellipticity are observed, which indicates negligible shifts in the secondary  
259 structure of the peptide in the presence of cerium ions. A slight decrease in ellipticity at 200 nm  
260 was observed in the scrambled peptide at 1000  $\mu$ M, which indicates an increase in random coil  
261 content at high cerium ion concentrations. Although, CD results could not quantify binding  
262 affinities of the designed peptides, the results indicate that the secondary structure of LanM1  
263 undergoes larger structural changes upon binding than the scrambled peptide. To understand this  
264 change, molecular dynamics simulations were performed, and conformational analysis of the  
265 peptides was carried out.



266

267 **Figure 2.** CD spectra of cerium (III) titration experiments with 100  $\mu\text{M}$  of (a) LanM1 peptide and  
 268 (b) scrambled LanM1 peptide in DI water at different cerium (III) concentrations up to 1000  $\mu\text{M}$ .

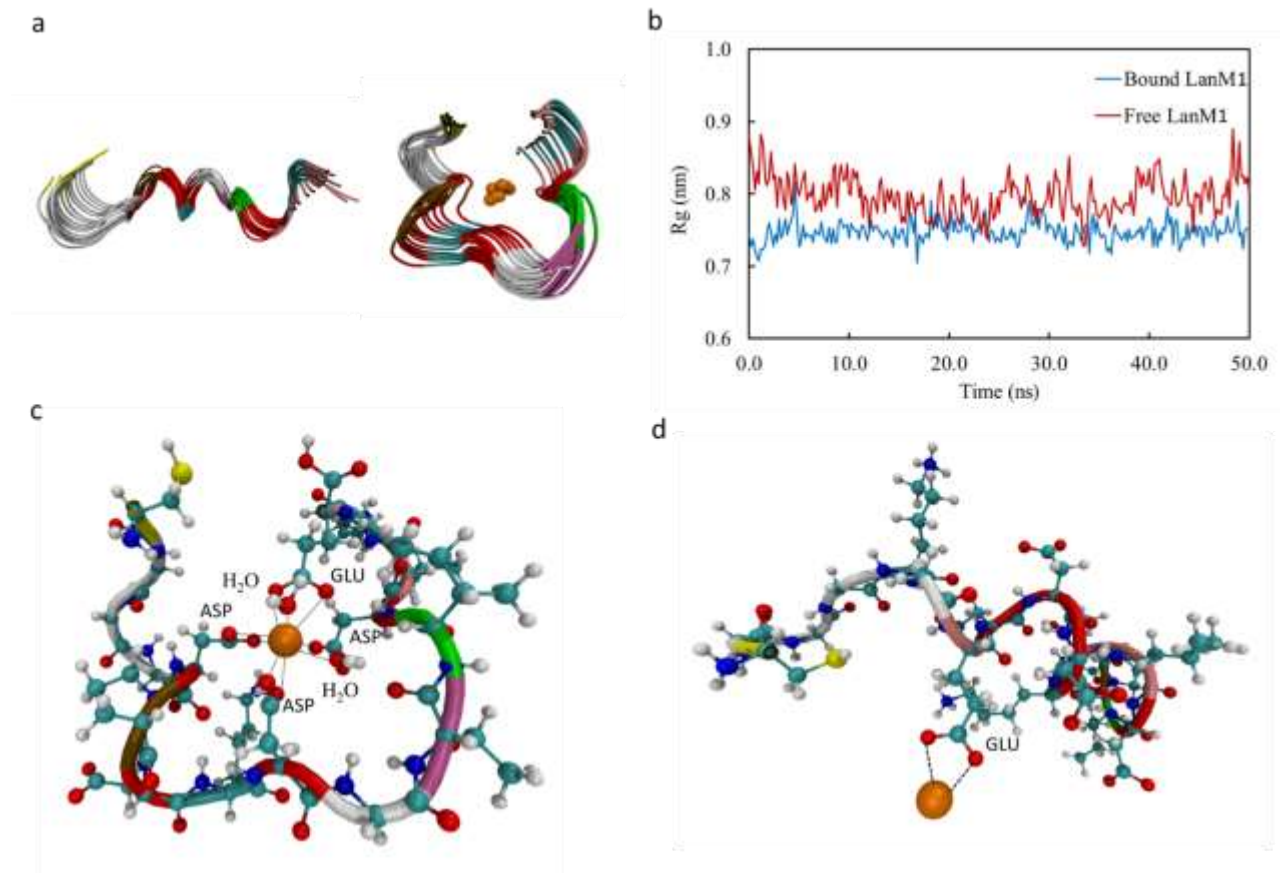
269 **Figure 3a** shows randomly selected superimposed MD snapshots of free LanM1, and LanM1-  
 270 cerium (III) complex taken from 50 ns long equilibrated trajectories. The visualization clearly  
 271 indicates a well-preserved and equilibrated structure of LanM1 before and after binding with the  
 272 ion. The snapshots illustrate a change in the conformation of the peptide upon binding that is

273 consistent with the CD results. To better understand the change in molecular conformation, radius  
274 of gyration of the peptide in bound and free states were calculated and reported in **Figure 3b**. The  
275 results show that the radius of gyration of free peptide is higher than bound peptide. We suspect  
276 that this might be due to the peptide being more open in free state and the structure becoming  
277 relatively rigid (packed) after complexation with cerium ion. The other possible interpretation  
278 could be that the pocket presents more affinity towards the ion than with water; hence the bound  
279 state configuration is maximizing the ion-peptide interaction over the ion-solvent interaction.  
280 These findings are consistent with Gutenthaler *et al.* who had done a similar binding investigation  
281 of europium (III) ions with the EF-hand loops of lanmodulin.<sup>24</sup>

282 To gain the atomistic details of the binding sites, **Figure 3c** shows the LanM1 binding site and the  
283 atoms that are coordinated with the Ce (III) ion. A total of nine oxygen atoms from LanM1 and  
284 water were observed to participate in the active binding site throughout the simulation. Out of  
285 these, seven were carboxylate oxygen atoms with five having an aspartic acid side chain and two  
286 having a glutamic acid side chain. The remaining two atoms were the oxygen atoms of water  
287 molecules near the binding site as shown in Figure 3c. Cook *et al.*, in their study determined the  
288 structure of all four metal-binding sites (EF-hand loops) of lanmodulin protein using NMR spectra  
289 when the binding sites were saturated with Y (III).<sup>43</sup> The atomistic investigation of the EF-hand  
290 loop I of lanmodulin bound to yttrium ions (the structure is available at protein data bank),<sup>43</sup> reveals  
291 that the binding site has nine oxygen atoms. However, in that case, no water molecules were  
292 associated in the binding site, defined as 2.3 Å distance from the ion. Gutenthaler *et al.* reported  
293 that the binding site for the Eu ion had a total of nine oxygen atoms with four atoms of aspartic  
294 acid and one of glutamic acid.<sup>24</sup> The remaining four oxygen atoms belong to the water molecules  
295 associated with the binding site. The number of water molecules coordinated in the inner sphere

296 of lanthanide ions decreases from nine to eight across the series (La  $\rightarrow$  Lu) due to the decreasing  
297 ionic radii. It has been found that the coordination number from La (III) to Nd (III) is nine, from  
298 Nd (III) to Tb (III) it is between nine and eight, and those from Tb (III) to Lu (III) have eight  
299 coordinated water molecules in the inner sphere.<sup>44</sup> In addition to coordination number, the average  
300 ion-H<sub>2</sub>O distance also varies with the atomic radii of REEs. For example, in case of Sm (III), the  
301 average ion-H<sub>2</sub>O distances is 2.474 Å and the value changes to 2.450 Å for Eu (III).<sup>44</sup> These factors  
302 together also impact the coordination chemistry of different ions when bound to the same binding  
303 site as found in different studies.<sup>24, 43, 45</sup> For example, in their study of lanthanide-dependent  
304 coordination interactions in lanmodulin, Liu *et al.* found that the coordination number of La (III)  
305 is 9.99 with the EF-1 hand loop of lanmodulin which changes to 9.00 in case of Lu (III).<sup>45</sup>

306 When a similar analysis on the scrambled LanM1 (**Figure 3d**) was performed, no such  
307 multidentate binding was observed. Instead, a weak interaction was found with the two oxygen  
308 atoms of the glutamic acid, which is in good agreement with the observation made by CD  
309 spectroscopy. To further probe LanM1 structure, an NMR study was conducted.



310

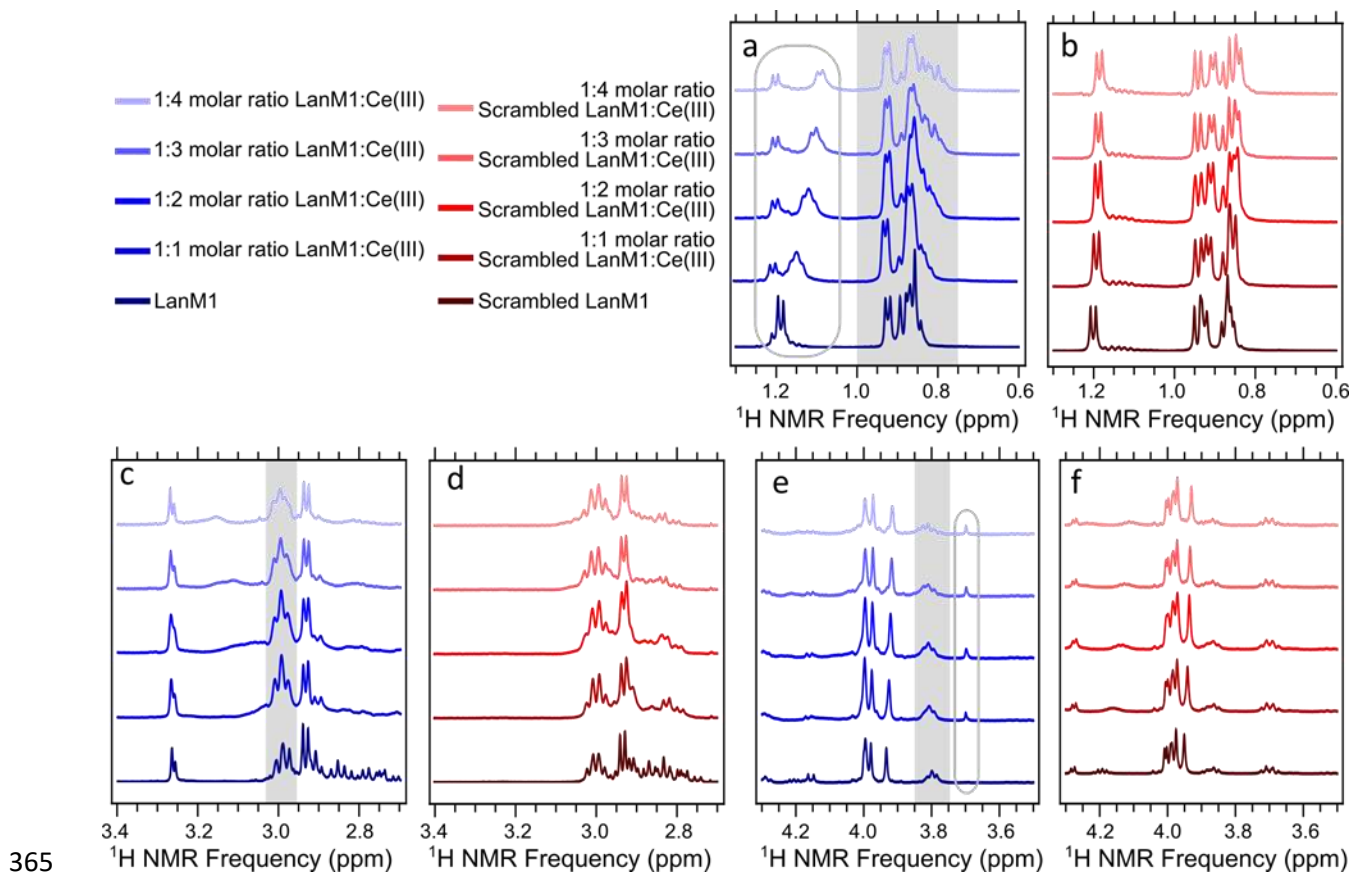
311 **Figure 3.** (a) Fifteen randomly selected superimposed MD snapshots of free LanM1 and cerium-  
 312 bound LanM1 from the trajectory upon equilibration. Rod representation with different colors  
 313 (same color scheme as in Figure 1) for amino acids is used for LanM1 and the cerium ion is  
 314 presented in orange color. The water molecules are not displayed for clarity. (b) Radius of gyration  
 315 (Rg) of the free (red) and ion-bound (blue) LanM1 in a 50 ns long simulation. (c) Coordination of  
 316 the cerium (III) ion with the LanM1 peptide after equilibration of molecular dynamics simulation.  
 317 A total of nine oxygen atoms are associated with the site. The cavity is formed with five oxygens  
 318 from aspartic acid side chains, two from a glutamic acid side chain and two water molecule oxygen  
 319 atoms. (d) Cerium ion binding site in scrambled LanM1 peptide after equilibration. Only two  
 320 oxygen atoms of glutamic acid are involved, resulting in a weak binding and no “pocket” in  
 321 comparison to LanM1.

322 <sup>1</sup>H solution NMR spectra of LanM1 and scrambled LanM1 at different NMR frequency ranges are  
323 shown side by side for comparison in **Figure 4**. We detect a greater effect to the spectra of LanM1  
324 compared to scrambled LanM1 as cerium (III) is added to the peptide solutions. We suggest that  
325 the sidechains within scrambled LanM1 may have transient interactions with the cerium (III) ions  
326 but not a cooperative binding effect that would result in distinct bound and unbound states. An  
327 additional control experiment conducted on polyproline, which does not bind to cerium (III),  
328 shows little to no change in <sup>1</sup>H NMR peaks and chemical shifts as cerium (III) is added (**Figure**  
329 **S2**).

330 As cerium (III) is added to LanM1, we observe broadening of peaks in the ranges of 0.75 to 1 ppm,  
331 2.95 to 3.05 ppm, and 3.75 to 3.85 ppm (gray highlighted regions in **Figures 4a, 4c, and 4e**). We  
332 observe less to the scrambled LanM1 sample as cerium (III) is added to the peptide solution  
333 (**Figures 4b, 4d, and 4f**). <sup>1</sup>H NMR peaks at the 0.75 to 1 ppm range can be assigned to the leucine  
334 and isoleucine methyl groups. We also note peak splitting for LanM1 at 1.05 ppm to 1.25 ppm in  
335 **Figure 4a**, which is within the <sup>1</sup>H NMR frequency range of the threonine methyl group.<sup>46</sup> Another  
336 difference in the NMR spectra is shown with the emergence of a new peak at ~ 3.7 ppm in the  
337 LanM1 sample that does not appear in the scrambled LanM1 sample (**Figure 4e and Figure 4f**).  
338 The linewidth of an NMR peak can be affected by the following factors when paramagnetic ions  
339 such as cerium (III) are involved: 1) distribution of conformations, 2) distance of the <sup>1</sup>H atom to  
340 the paramagnetic ion, and 3) dynamics, e.g., binding/unbinding of the ion, flipping between  
341 distinct conformations, and lifetimes of bound and unbound states.<sup>47</sup> When a <sup>1</sup>H atom is within  
342 spatial proximity consistent with peptide binding to the unpaired electron in cerium (III), electron-  
343 nuclear interaction is likely to be the dominant factor in peak broadening and shifting.  
344 Furthermore, we expect peak broadening to increase as <sup>1</sup>H atoms get closer to the unpaired

345 electron. For the  $^1\text{H}$  atoms closest to the electron, peak broaden may make the NMR signal difficult  
346 to detect; for example: in **Figure 4c**, we see a “baseline roll” between 3.0 to 3.2 ppm, suggesting  
347 the presence very broad NMR signals. Hence, the changes to the  $^1\text{H}$  chemical shifts of the residues  
348 that are closer to the cerium (III) ion and directly participate in ion binding may be difficult to  
349 detect, creating what is known as “dark-states” in NMR spectroscopy.<sup>47</sup> The peak broadening and  
350 shifting we highlight in **Figures 4a, 4c, and 4e** is more detectable because they correspond to  
351 weaker electron-nuclear interactions, providing information about the residues that may not  
352 directly participate in cerium (III) binding and are farther from the binding site. We interpret the  
353 peak broadening in **Figures 4a, 4c and 4e** to be a result of multi-site occupancy between structural  
354 conformations that produce multiple peaks per atomic site (though they may overlap). In **Figure**  
355 **4a**, we observe peak splitting rather than peak broadening at 1.2 ppm because the peptide adopts  
356 two different conformations with a larger chemical shift difference and no spectral overlap. The  
357 phenomenon of “pseudocontact shifts” induced by lanthanides is likely to be relevant here.<sup>48-50</sup>  
358 The emergence of a new peak in **Figure 4e** indicates a new conformation that only occurs in the  
359 presence of the cerium (III) ion. Further NMR experiments can provide more information about  
360 the precise interactions involved between the peptide residues and cerium (III) ions. Overall, our  
361 data support the conclusion that LanM1 binds to cerium (III), confirming CD and MD simulation  
362 results. In contrast, scrambled LanM1 has the same sidechains as LanM1, but does not bind cerium  
363 (III), indicating the importance of the amino acid sequence.

364

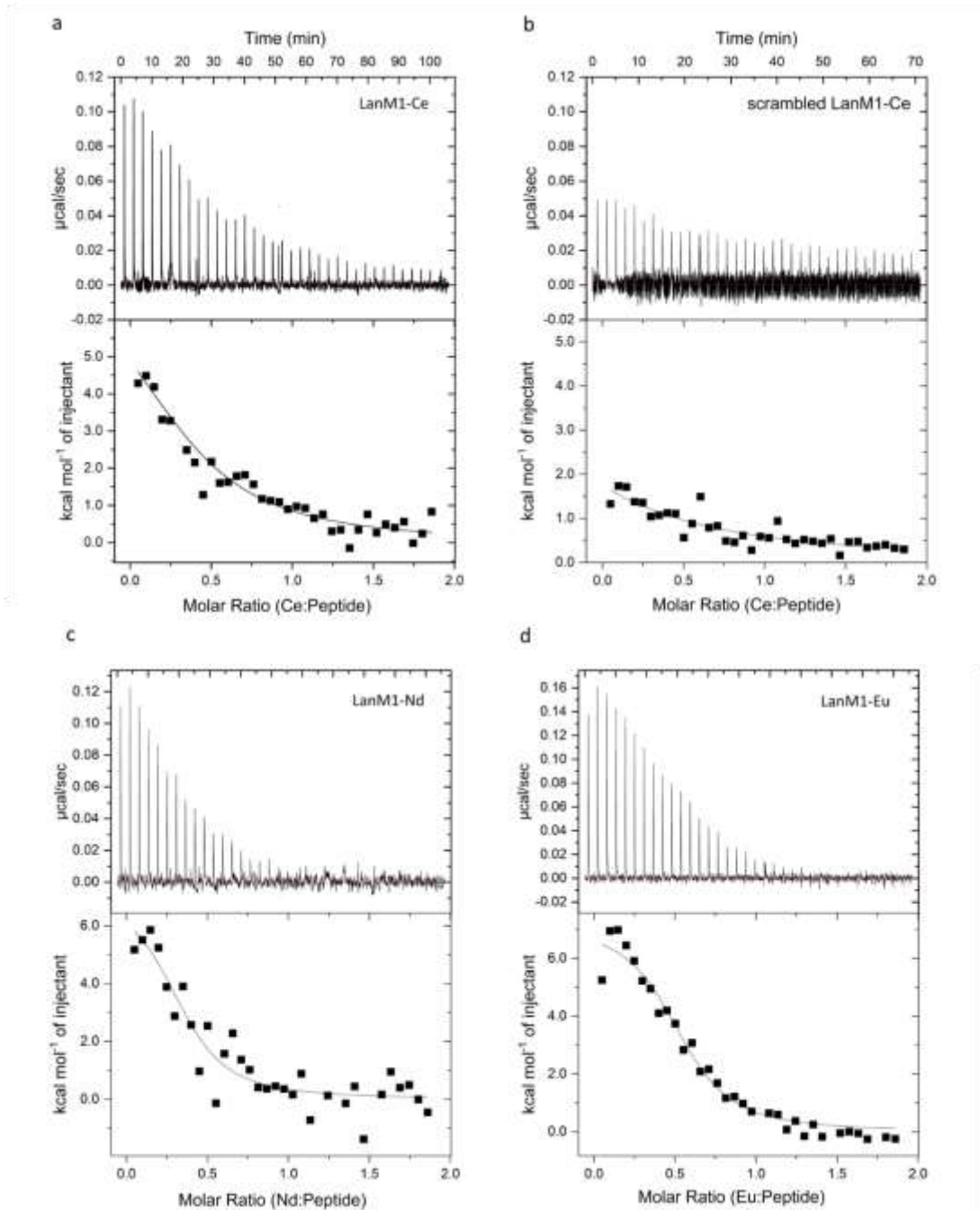


365  
 366 **Figure 4.**  $^1\text{H}$  NMR measurements of LanM1 peptide and scrambled LanM1 peptide at different  
 367 molar ratios of peptide to cerium (III). Panel a, c, and e show the NMR spectra of of LanM1 in  
 368 blue (the shade gets lighter with increasing cerium concentration from zero to 1:4 molar ratio).  
 369 The NMR spectra for scrambled LanM1 is shown in red (the shade gets lighter with increasing  
 370 cerium concentration from zero to 1:4 molar ratio) Panels b, d, and f. Gray highlighted regions in  
 371 Panels a, c, and e identify peaks which experience line broadening as more cerium is added to the  
 372 LanM1 peptide. Gray encircled regions identify peak splitting or the emergence of new peaks.

### 373 **Thermodynamic Properties of Binding in Solution**

374 To better understand and elucidate the binding affinity, isothermal titration calorimetry was  
 375 conducted to estimate thermodynamic properties of binding for various REEs (Ce (III), Nd (III),

376 Eu (III), and Y(III)) at 303.15 K. In addition, experiments on scrambled LanM1 with cerium (III)  
377 ions were conducted to serve as comparison. **Figure 5a and b** show the cerium titration curves  
378 (raw data), isotherm and one site-binding model fit for LanM1 and scrambled LanM1,  
379 respectively. The titration results for neodymium and europium ions with LanM1 are provided in  
380 **Figure 5c and d**, respectively. LanM1 had low affinity for Y(III) ions making thermodynamic  
381 properties difficult to estimate. ITC raw data, Wiseman plot, and one-site binding model fit for  
382 yttrium with LanM1 is provided in **Figure S3**.



383

384 **Figure 5.** ITC raw data, Wiseman plot and one-site binding model fit for (a) LanM1 with cerium  
 385 (III) ions (b) scrambled LanM1 with cerium (III) ions (c) LanM1 with neodymium (III) ions (d)  
 386 LanM1 with europium (III) ions. In all experiments, the peptides were in the cell at 20.0  $\mu\text{M}$  and

387 the ions were in the syringe at a concentration 200.0  $\mu\text{M}$ . The experiments were performed at 30  
388  $^{\circ}\text{C}$  using ultrapure water.

389 At a given temperature, the change in enthalpy ( $\Delta\text{H}$ ), and change in entropy ( $\Delta\text{S}$ ) determine the  
390 sign and magnitude of the binding free energy using the expression  $\Delta\text{G} = \Delta\text{H} - T\Delta\text{S}$ . The estimated  
391 thermodynamic properties of binding for Ce (III), Nd (III), and Eu (III) with LanM1 and Ce (III)  
392 with the scrambled LanM1 are reported in **Table 1**. In the case of cerium (III) binding with LanM1,  
393 the change in enthalpy ( $\Delta\text{H}$ ) and entropy ( $\Delta\text{S}$ ) were measured to be  $6.66 \pm 1.32$  kcal/mol and  $46.85$   
394  $\pm 3.54$  cal/mol K, respectively, and used to obtain the binding free energy ( $\Delta\text{G}$ ) of  $-7.50 \pm 0.31$   
395 kcal/mol. The dissociation constant  $K_d$  was estimated to be  $3.84 \pm 1.47$   $\mu\text{M}$  which is comparable  
396 to similar investigations of cerium (III) via ITC using a different peptide sequence that was derived  
397 from calmodulin.<sup>16, 24, 51</sup> A negative  $\Delta\text{G}$  is an indication of spontaneous binding. The process is  
398 enthalpically disfavored with the increase in entropy driving the process. For scrambled LanM1,  
399  $K_d$  was estimated to be  $20.59 \pm 5.84$   $\mu\text{M}$ , nearly an order of magnitude higher.

400 The obtained  $K_d$  values for neodymium and europium ions with LanM1 were  $1.44 \pm 0.07$   $\mu\text{M}$  and  
401  $0.80 \pm 0.48$   $\mu\text{M}$ , respectively. The dissociation constants were correlated to the ionic radius of  
402 REEs as shown in **Figure S4** where  $K_d$  increases as the ionic radius increases. Nitz *et al.*<sup>52</sup> studied  
403 the binding affinity of REEs with lanthanide-binding tags (LBTs) and found a non-monotonic  
404 change in  $K_d$  with the ionic radius. The minimum  $K_d$  of  $57 \pm 3$  nM was observed for Tb (III) that  
405 has an atomic radius of  $\sim 1.04$  Å. In light REE range, the  $K_d$  increased with the ionic radius  
406 consistent with our results. Similar results were found in the calmodulin protein.<sup>53</sup>

407 The ITC results for potential competitor ions calcium (Ca (II)) and copper (Cu (II)) with LanM1  
408 are reported in **Figure S5**. It was found that LanM1 does not bind with copper and calcium ions,  
409 consistent with the similar investigation in which lanmodulin protein was immobilized onto

410 agarose microbeads and was studied for its affinity towards several REEs and non-REEs by Dong  
 411 *et al.*<sup>22</sup> In an investigation of the four EF-hand loop peptides of the lanmodulin protein by  
 412 Gutenthaler *et al.*<sup>24</sup> the peptide showed no affinity towards calcium ion. In a study by Hussain *et*  
 413 *al.*<sup>21</sup> of a thermo-responsive genetically encoded elastin-like polypeptide that has an REE-binding  
 414 domain (lanmodulin) it was found that the polypeptide did not bind to copper and zinc ions, further  
 415 supporting our findings. The results are also in agreement with Wei and co-workers<sup>23</sup> who found  
 416 lanmodulin protein immobilized to magnetic nanoparticles (MNP-LanM) did not adsorb non-  
 417 REEs.

418 **Table 1.** Estimated thermodynamic properties for LanM1 binding with cerium (III), neodymium  
 419 (III) and europium (III) ions using isothermal titration calorimetry (ITC). Results for the scrambled  
 420 LanM1 with cerium (III) are also reported. The experiments were conducted at 30°C and pH was  
 421 between 5.0 to 5.5. Data are represented by the average  $\pm$  the standard deviation for n=3 repeats.

Peptide	REE Ion	Association Constant $K_a$ ( $\mu\text{M}^{-1}$ )	Dissociation Constant $K_d$ ( $\mu\text{M}$ )	$\Delta H$ (kcal/mol)	$\Delta S$ (cal/mol K)	$\Delta G$ (kcal/mol)
LanM1	Ce	$0.30 \pm 0.13$	$3.84 \pm 1.47$	$6.66 \pm 1.32$	$46.85 \pm 3.54$	$-7.50 \pm 0.31$
LanM1	Nd	$0.70 \pm 0.03$	$1.44 \pm 0.07$	$6.10 \pm 1.51$	$48.15 \pm 3.04$	$-8.09 \pm 0.03$
LanM1	Eu	$1.47 \pm 0.80$	$0.80 \pm 0.48$	$6.84 \pm 5.09$	$50.60 \pm 0.57$	$-8.49 \pm 0.34$
Scrambled LanM1	Ce	$0.05 \pm 0.01$	$20.59 \pm 5.84$	$13.11 \pm 4.74$	$64.63 \pm 15.61$	$-6.47 \pm 0.25$

422

423 We also tested LanM1 binding affinity with cerium (III) at low pH conditions. The studies at low  
 424 pH conditions are relevant to coal mine drainages where the discharges are at low pH (<5).<sup>54</sup> ITC  
 425 experiments at three pH conditions 2.0, 3.0 and 3.5 were performed (**Figure S6**). It was found that  
 426 there was no binding at pH 2.0. However, the titration curves at pH 3.0 and 3.5 show increasingly  
 427 distinct changes in energy during the first few injections, indicating increasing binding affinity.  
 428 This suggests free peptide could be regenerated by lowering the pH to release the ions. In recent  
 429 work by Dong *et al.*<sup>22</sup> desorption studies were performed on agarose beads with grafted lanmodulin

430 protein in which the effect of pH was investigated. It was found that immobilized lanmodulin can  
431 effectively bind Nd (III) ions down to pH 2.4. However, further lowering the pH to 2.2 resulted in  
432 a 50% drop in binding and it became insignificant below pH 1.7. Our results also agree with  
433 Gauthier *et al.*,<sup>19</sup> who showed that solubilized lanmodulin protein retains REE binding affinity  
434 down to around pH 2.5. The pKa of aspartic acid and glutamic acid are ~3.9 and ~4.3, respectively  
435 so below this pH range, the peptide loses its negatively charged groups and might contribute to  
436 low affinity for REEs below pH 2.5.

### 437 **Binding Analysis of Immobilized Peptides**

438 To understand binding affinity of the immobilized peptide with some REEs and competing non-  
439 REEs, quartz crystal microbalance with dissipation (QCM-D) analysis was performed. In a typical  
440 QCM-D experiment, ultrapure water is introduced on the gold sensor to generate a baseline. Once  
441 a stable baseline is established, peptide solution of known concentration is introduced and a  
442 negative shift in frequency observed which is proportional to the hydrated mass loading of the  
443 peptide on the surface. Rinses are often employed to remove weakly bound molecules. In addition  
444 to frequency, dissipation is measured – which provides information about the energy loss and gives  
445 an indication of the viscoelastic properties. If there is no significant shift in dissipation, the layer  
446 is rigid, otherwise, the layer is viscoelastic.<sup>55</sup> After the desired peptide is immobilized on the gold  
447 surface, and an ultrapure water rinse is performed, REE binding on the immobilized peptide is  
448 done by allowing an REE solution of known concentration to flow over the surface. Then, another  
449 round of ultrapure water rinsing is performed to remove weakly bound REE. In this study, the  
450 amount of REE that binds to the peptide isn't enough to illicit a significant shift in frequency.  
451 Therefore, after ultrapure water rinsing, 1 mM sodium phosphate solution is allowed to flow over  
452 the surface and bind to surface-bound REEs as a way to quantify the amount of REE bound. This

453 technique using phosphate was confirmed by using it to estimate the  $K_d$  of a peptide derived from  
454 calmodulin, and was found to be similar to our previous work (**Figure S7<sup>16</sup>**). During LanM1  
455 peptide loading, there was no significant changes in dissipation observed, resulting in a rigid layer  
456 formation and thus Sauerbrey model was sufficient to estimate the mass loading. However, a  
457 viscoelastic layer was formed upon phosphate loading and the Voigt model<sup>56</sup> was used to estimate  
458 the mass loading.

459 All surface binding studies were conducted assuming the peptide binding to REE was a reversible  
460 process as shown by **Equation 1**:

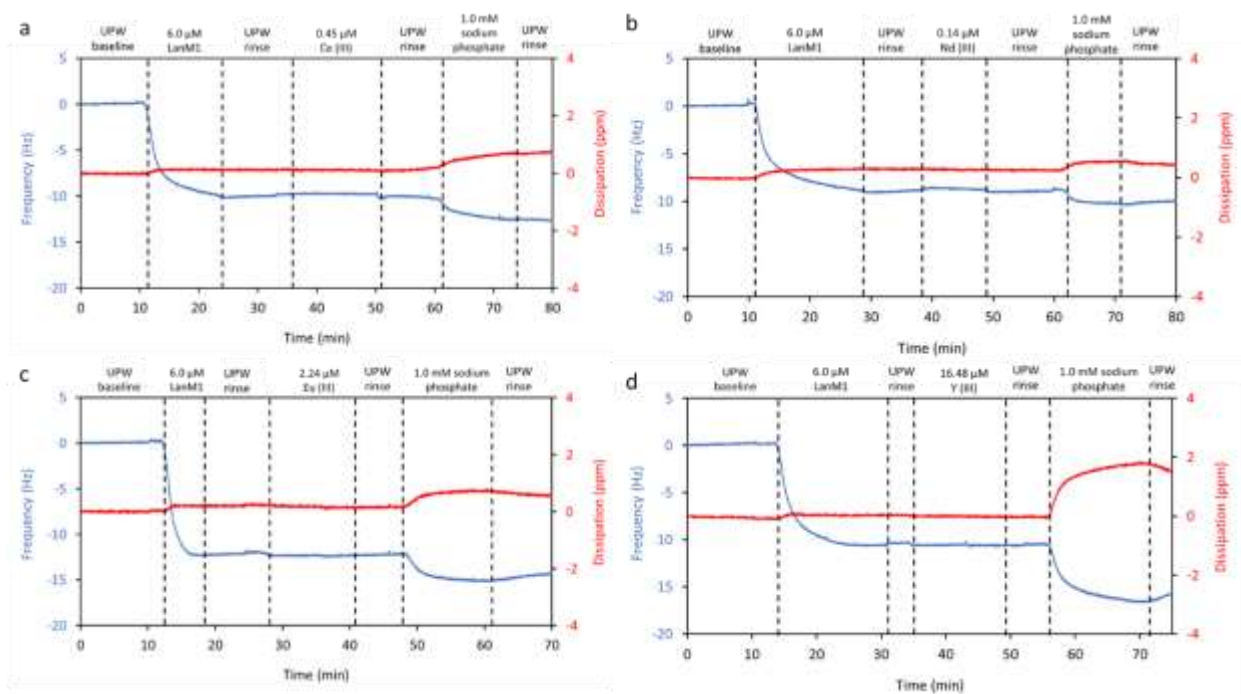


462 Where  $k_f$  represents the forward rate constant and  $k_r$  is the reverse rate constant. The binding  
463 affinity,  $K_d$  is then defined as the ratio  $k_r/k_f$ .  $K_d$  is a dissociation constant and is the reciprocal of  
464 the association constant  $K_a$  which is often reported for ligand-ion complexation. The linearized  
465 slope of binding for a peptide-REE-phosphate system as shown in **Note S1** is found to be identical  
466 to that of a peptide-REE system. When tested with calmodulin peptides, we see that the  $K_d$   
467 estimated from phosphate addition was 1.6  $\mu\text{M}$  as shown in **Figure S7** which is around what was  
468 previously reported (1.3  $\mu\text{M}$ <sup>16</sup>). We assume that the amount of phosphate bound is proportional to  
469 the amount of cerium bound on the surface of the QCM sensor. To ensure phosphate does not  
470 interact with the lanmodulin peptides, control experiments were conducted where no binding was  
471 observed, shown in **Figure S8**. Our previous study shows that when no peptide was present on  
472 the QCM sensor, no irreversible binding was observed for phosphate<sup>17</sup> – indicating all phosphate  
473 binding seen is due to interactions with peptide-cerium films. We also observed that higher LanM1  
474 loading on gold sensor (frequency change  $\sim 15$  Hz or greater) will result in minimal REE binding as

475 shown in **Figure S9**. Thus, it is critical to control the loading of the peptide on the surface to  
476 maintain peptide affinity. This observation suggests that the density of the peptides on a surface  
477 plays a role in ion binding. In solution, the peptides are freely suspended at low concentrations.  
478 Whereas peptides tethered to a surface or particle are more crowded and we speculate the crowding  
479 of peptides on a surface may cause changes in the peptide secondary structure thereby altering the  
480 binding pocket, changes to water organization around the peptide, steric hinderance, or interaction  
481 of peptides with each other. Therefore, depending on the peptide density on the surface, the trends  
482 in peptide-ion affinity may be different for a surface immobilized peptide than a peptide in  
483 solution. Any changes to trends in affinity will manifest in the peptide selectivity for REEs over  
484 non-REEs or one REE over another.

485 **Figure 6a-d** show QCM-D results for gold-immobilized LanM1 exposed to Ce (III), Nd (III), Eu  
486 (III) and Y(III) ion, respectively. **Figure 6** displays experiments performed at the lowest REE  
487 concentrations where binding was observed where the blue line corresponds to the frequency shift,  
488 while the red line corresponds to the dissipation shift. Ultrapure water served as the baseline for  
489 the experiment, which was immediately followed by a 6.0  $\mu\text{M}$  peptide solution. An experiment  
490 exposing gold-immobilized scrambled LanM1 to Ce (III) is shown in **Figure S10**. In the case of  
491 LanM1 and scrambled LanM1, frequency shift upon addition of phosphate ions was observed  
492 down to 0.45  $\mu\text{M}$  Ce (III), with much less binding occurring in the case of the scrambled LanM1.  
493 These results are consistent with bulk investigations using CD, NMR, ITC and molecular dynamics  
494 results showing scrambled LanM1 having lower affinity for cerium (III) than LanM1. In the case  
495 of Nd (III), Eu (III) and Y (III), the lowest concentrations binding was observed at was 0.14  $\mu\text{M}$ ,  
496 2.24  $\mu\text{M}$  and 16.48  $\mu\text{M}$ , respectively.

497 Non-REE ions are also known to complex with phosphate and when using solubility product  
498 constant as an rough indication of the affinity of the ions for phosphate, Ca (II), and Cu (II) will  
499 have at least as high of an affinity when compared to cerium (III).<sup>57</sup> Therefore, similar QCM-D  
500 experiments were performed with two non-REE Ca (II) and Cu (II) competitor ions. The results of  
501 surface-bound LanM1 peptide with these ions are provided in **Figure S11**. Like the bulk, LanM1  
502 peptide does not show affinity for either calcium or copper ions. Even at a higher competitor ion  
503 concentration of 29.0  $\mu\text{M}$ , no change in the frequency was observed.



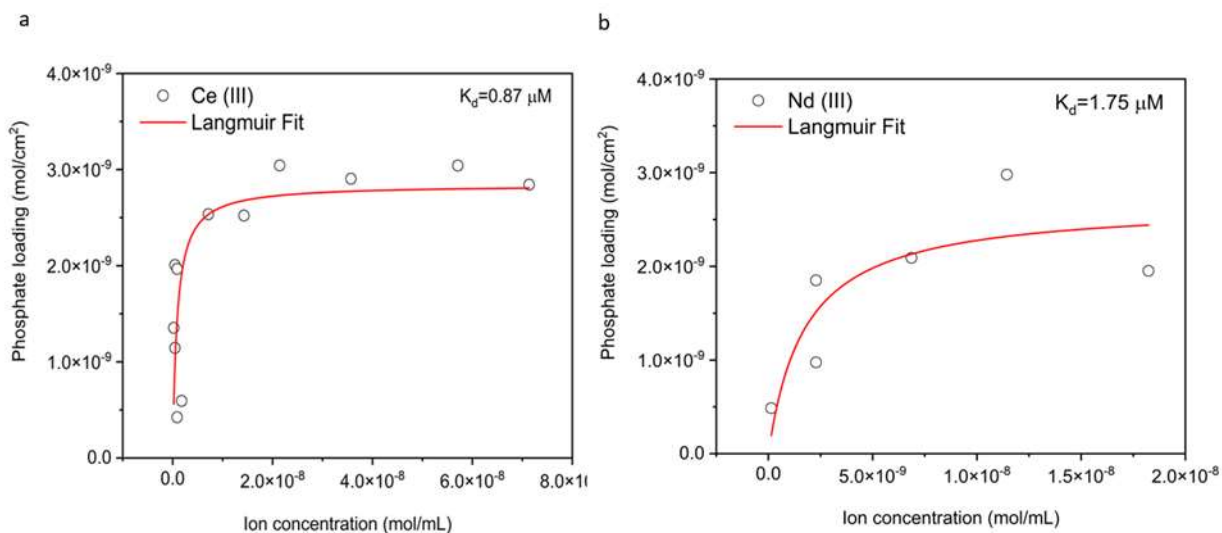
504  
505 **Figure 6.** Frequency and dissipation shifts measured using a quartz crystal microbalance (QCM-  
506 D) for (a) cerium (III), (b) neodymium (III), (c) europium (III), and (d) yttrium (III) adsorption on  
507 LanM1. The dashed lines show when the solution was changed, and the labels within the lines  
508 show the solution being during that time. The blue line corresponds to the frequency shift, and the  
509 red line corresponds to the dissipation shift. The 9<sup>th</sup> overtones are shown.

510 QCM-D experiments were performed at various REE ion concentrations to estimate surface-bound  
511 LanM1 dissociation constants for Ce (III) and Nd (III). In acid mine drainage, the concentration  
512 of Ce (III) and Nd (III) is the highest among other REEs<sup>58</sup> which makes this pair of particular  
513 interest for that application. The Langmuir adsorption isotherm model was fit to phosphate loading  
514 data at different REE concentration in QCM-D experiments to describe the adsorption process.<sup>59,</sup>  
515 <sup>60</sup> Although, it is an ideal model that may not fully capture the complexity of adsorption, it can still  
516 provide valuable insights into adsorption behavior. The model is given as:

517  
518 
$$q_e = \frac{R_T C_e}{C_e + K_d} \quad (2)$$

519  
520 where  $q_e$  is phosphate loading ( $\text{mol}/\text{cm}^2$ ),  $R_T$  ( $\text{mol}/\text{cm}^2$ ) is the Langmuir constant related to  
521 maximum phosphate loading,  $K_d$  ( $\text{mol}/\text{ml}$ ) is the dissociation constant, and  $C_e$  ( $\text{mol}/\text{ml}$ ) is the  
522 equilibrium bulk concentration of the ions. In this work, non-linear regression was performed using  
523 OriginLab software to fit the data. The removal of one outlier was allowed for each ion data set.

524 **Figure 7** shows the change in phosphate loading (proportional to REE loading) with ion  
525 concentration for cerium (III) and neodymium (III) along with Langmuir fitting. Surface bound  
526 LanM1 dissociation constants ( $K_d$ ) of  $\sim 0.9 \mu\text{M}$  and  $\sim 1.8 \mu\text{M}$  were obtained for cerium (III) and  
527 neodymium (III), respectively. Details of the non-linear fitting are provided in **Table S1**. When  
528 compared with the bulk results, it is found that the affinity for cerium (III) ions increases upon  
529 immobilization. Because of the high error, it is difficult to determine if there is a shift for Nd (III)  
530 upon peptide immobilization. However, these results show for the first time that surface-bound  
531 LanM1 peptides bind REEs, and motivates future studies to explore how immobilization impacts  
532 the trends in  $K_d$ .



533  
 534 **Figure 7.** Binding of (a) Ce (III) and (b) Nd (III) ions to gold-immobilized LanM1 peptides where  
 535 phosphate is proportional to REE binding. In both cases, a simple Langmuir adsorption model was  
 536 fit to estimate the K<sub>d</sub>. Open circles represent experimental data points whereas the red lines show  
 537 the Langmuir fit. Estimated K<sub>d</sub> values are shown in the respective panels.

### 538 Selectivity Analysis of Immobilized Peptides

539 In a practical separation scheme, immobilized peptides are exposed to a mixture of REEs.  
 540 Separation occurs if the peptide has a higher affinity (lower K<sub>d</sub>) for one REE over another due to  
 541 the preferential partitioning of the REE ion on to the solid peptide-containing phase. For dilute  
 542 solutions, selectivity can be approximated using a ratio of association constants ( $K_a = 1/K_d$ ) where  
 543 the ideal selectivity is represented as  $\alpha_{1/2} = K_{a1}/K_{a2}$ , and 1 and 2 represent different metal species.<sup>61</sup>  
 544 Since  $\alpha_{1/2}$  is based on the association reaction,  $\alpha_{1/2} > 1$  indicates a higher affinity for species 1.  
 545 Higher values of  $\alpha_{1/2}$  indicate higher degrees of separation between the two ions. The selectivity  
 546 of the LBT peptide, LanM protein, and LanM1 peptide for Nd over Ce are summarized in **Table**  
 547 **2**. Typically, selectivity for neighboring lanthanides is compared; however, the Nd/Ce ion pair was  
 548 selected to enable the comparison with this work. Two non-biological ligands are included as these

549 are the leading commercial extractive resins for REE separations: DGA-linear and DGA-branched  
 550 (Eichrom Technologies, Ltd.). A key distinguishing factor between the bio-derived ligands and the  
 551 DGAs are the solution conditions under which selectivity is achieved. DGA-linear and DGA-  
 552 branched resin exhibit selectivity for one REE over another REE at high acid concentrations < pH  
 553 1 whereas the bio-derived ligands exhibit selectivity in more moderate pH solutions, i.e. > pH 3.  
 554 The  $K_a$ ,  $k'$  and  $K_d$  values used to construct **Table 2** are in **Tables S2** and **S3** of the **SI**.

555 **Table 2.** Calculated ideal selectivity for DGA resins, LBT peptide, LanM protein, and LanM1  
 556 peptide for selected REE pairs.

Ligand, Support	Matrix	Ion Pair	Selectivity ( $K_{a1}/K_{a2}$ ) or ( $k'_1/k'_2$ )	$K_a$ or $k'$ Reference
DGA-branched, resin	1 M HNO <sub>3</sub>	Nd/Ce	1.8	Horwitz 2005 <sup>62</sup>
DGA-linear, resin	0.05 M HNO <sub>3</sub>	Nd/Ce	4.1	Horwitz 2005 <sup>62</sup>
LanM protein, unsupported	pH 5, 100 mM KCl	Nd/Pr	0.5	DeBlonde 2020 <sup>*19</sup>
LBT, unsupported	pH 7.0, 10 mM HEPES, 100 mM NaCl	Nd/Ce	3.5	Nitz 2004 <sup>52</sup>
LanM1, unsupported	pH 5.4, ultrapure water	Nd/Ce	2.0	This Work
LanM1, on gold	pH 5.4, ultrapure water	Nd/Ce	0.5	This Work

557 \*Ce data was not available therefore Pr selectivity is reported instead.

558 \*\* $k'$  is proportional to the  $K_a$

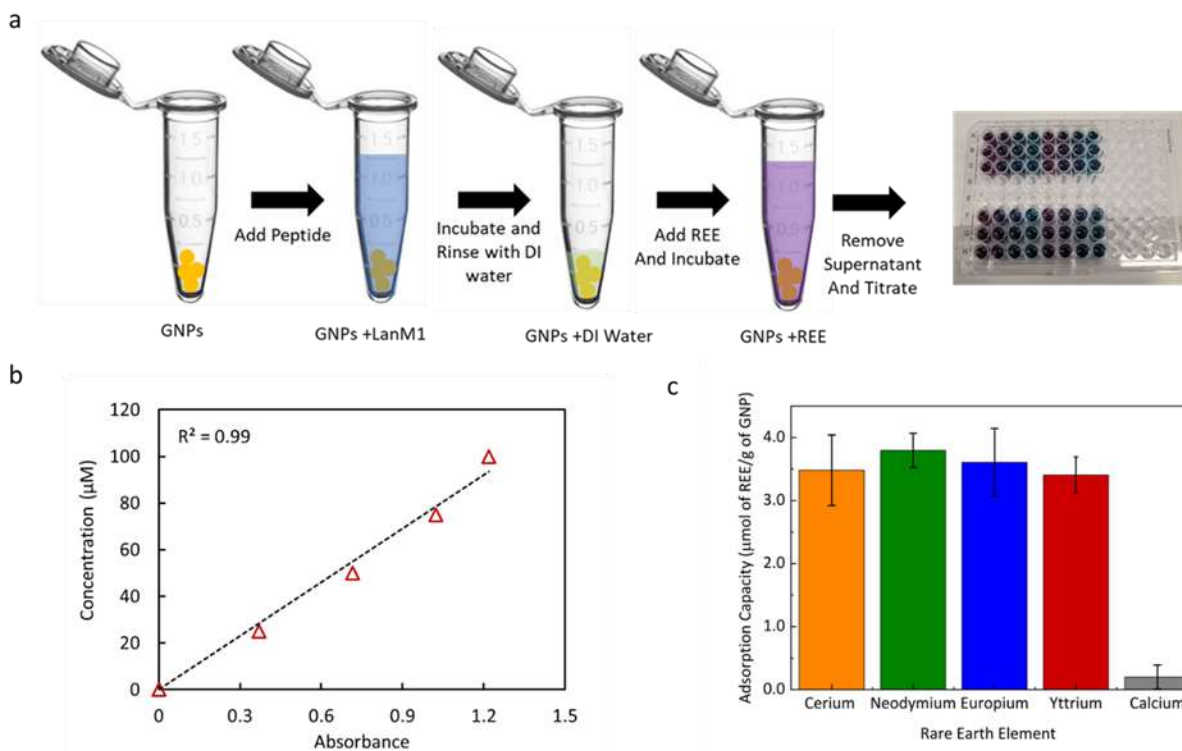
559  
 560 A common challenge when comparing association and dissociation constants ( $K_a$  and  $K_d$ ) across  
 561 the literature is the wide variation of matrices used for binding (pH, ionic strength, buffer, or acid  
 562 type) and the ions tested. For this reason, the discussion herein will refer to general trends and  
 563 order of magnitude differences. Recognizing the caveat that the lanmodulin protein data in **Table**  
 564 **2** represents a more challenging separation of neighbors Pr/Nd than Nd/Ce—both LBT and LanM1  
 565 peptides in solution exhibit selectivity that is on par with the LanM protein: 3.5, 2.3, and 2.0,  
 566 respectively. This is interesting because the  $K_d$  of LanM protein is 6 orders of magnitude lower  
 567 than the LBT and LanM1 peptides. Recall, the  $K_d$  for LanM protein across the lanthanide series

568 ranges from 0.4 to 10 pM;<sup>19</sup> the  $K_d$  for the LBT peptide ranges from 0.057 to 3.5  $\mu\text{M}$ ;<sup>52</sup> and the  $K_d$   
569 for solution phase LanM1 in this work ranges from 0.8 to 3.8  $\mu\text{M}$ . Thus, high affinity does not  
570 necessarily correlate to high selectivity between the tested REEs.

571 Common ligands for lanthanide separations such as EDTA, DOTA, and DTPA exhibit a  
572 monotonic increase in affinity as the atomic number and charge density increase across the  
573 lanthanide series<sup>63</sup> known as the size selectivity trend. Specialty macrocyclic ligands like macropa  
574 exhibit a reverse size selectivity trend where the affinity decreases monotonically as the atomic  
575 number and charge density increase across the lanthanide series.<sup>64</sup> The lanmodulin protein exhibits  
576 a dual selectivity in which an inflection point in dissociation constant occurs at Sm. The selectivity  
577 trend of the LBT peptide is more consistent with the traditional ligands as the affinity increases  
578 with increasing atomic number for the light lanthanides, La  $\rightarrow$  Eu. The LBT peptide shows  
579 negligible selectivity between the heavier lanthanides, Eu  $\rightarrow$  Lu. Based on the first three  
580 lanthanides tested in this series, the LanM1 peptide exhibits the traditional size selectivity trend in  
581 solution, **Table 1**. Further investigation of dissociation constants with heavier lanthanides will be  
582 necessary to discern the full extent of the selectivity trend for LanM1 in solution. Based on the  
583 first two tested lanthanides (Nd and Ce) for immobilized LanM1, the selectivity trend may reverse  
584 or exhibit non-traditional behavior when LanM1 is bound to particular surfaces, as observed in  
585 this study.

### 586 **Binding Investigation on Gold Nanoparticles (GNPs)**

587 The potential to use surface-bound LanM1 in REE separation is demonstrated by immobilizing  
588 LanM1 peptide on gold nanoparticles (diameter <100 nm) and subsequently estimating the  
589 adsorption capacity of peptide-immobilized GNPs as shown in **Figure 8a**.



590  
591 **Figure 8.** (a) Pictorial representation of the step-by-step procedure used to make peptide-bound gold  
592 nanoparticles (GNPs) and analyze REE binding capacity. (b) The calibration curve for Ce (III)  
593 ions based on the UV-visible absorption spectra. (c) A comparison of the adsorption capacities  
594 ( $\mu\text{mol REE/g GNP-LanM1}$ ) for different REEs and negligible adsorption of calcium (II) ions.  
595 After peptide functionalization GNPs were incubated with REE containing solution, then the GNPs  
596 were separated from the supernatant and titrated with arsenazo III reagent. The absorption at 655  
597 nm wavelength was measured and used to generate a calibration curve like that shown in **Figure**  
598 **8b**, from which the concentration of sample supernatant was estimated. **Figure 8b** shows an  
599 example calibration curve for Ce (III) ions and calibration curves for Nd (III), Eu (III), and Y (III)  
600 and Ca (II) ions can be found in **Figure S12**. UV-visible absorption spectra of known cerium  
601 concentration solutions titrated against arsenazo III reagent used to generate the calibration curve  
602 is provided in **Figure S13**.

603 The adsorption capacity ( $\mu\text{mol-REE/g-GNP-LanM1}$ ) was calculated using **Equation 3**:

$$604 \quad Q_e = \frac{(C_0 - C_e) \times V}{m} \quad (3)$$

605 where  $C_0$  is the initial REE concentration ( $\mu\text{M}$ );  $C_e$  is the REE concentration of the supernatant;  $V$   
606 is the volume in the vial (L), and  $m$  is the mass of the GNP-LanM1 (g).

607 Several equilibrium adsorption experiments of LanM1-GNPs at different concentrations were  
608 performed for REEs Ce (III), Nd (III), Eu (III), and Y (III) and non-REEs Ca (II) and the estimated  
609 the adsorption capacity for the ions at different concentrations are reported in **Table S4**. A  
610 comparison of average equilibrium adsorption capacities of REEs and competing non-REE  
611 calcium (II) ion is shown in **Figure 8c**. These values for REEs are assumed to be the saturated  
612 adsorption capacity since saturation appears to occur at concentrations tested (see **Table S4**). The  
613 results show LanM1 grafted GNPs do not adsorb calcium ions. These findings align well with ITC  
614 and QCM-D results in this study and are consistent with similar investigations.<sup>22, 24</sup> The REE  
615 saturated adsorption capacities of GNP-grafted LanM1 for Ce (III), Nd (III), Eu (III), and Y (III)  
616 are similar,  $\sim 3.5 \mu\text{mol}$  of REE per g of GNP-LanM1, further supporting that concentration range  
617 is above the saturation point for these REE ions.

618 In a recent study of lanmodulin-functionalized magnetic nanoparticles for REE recovery, the  
619 saturated adsorption capacity of  $5.46 \pm 0.46 \mu\text{mol-Tb/g-MNP}$  was reported. The experiment was  
620 performed using 20 mM 2-(N-Morpholino)-ethanesulfonic acid (MES) buffer at pH 5.0 with 2.5  
621 mg/ml of MNP-LanM and  $\sim 62.93 \mu\text{M}$  Tb (III),<sup>23</sup> which has some similarities to our experiment  
622 in DI water at pH 5.0-5.5 with 5-8 mg GNP/mL and 20 to 125  $\mu\text{M}$  REE, serving as a useful  
623 comparison. In their study, loading on MNPs was  $2.67 \pm 0.15 \mu\text{mol LanM SpyCatcher/g-MNP}$ .  
624 We roughly estimated the molar loading of LanM1 to be  $\sim 3.74 \mu\text{mol LanM1/g-GNP}$  based on our

625 QCM-D mass estimates, noting that our estimate is likely and overestimate because we did not  
626 account for water. The results in QCM-D experiment show a minimum dissipation during peptide  
627 loading which indicates a rigid layer formation and low water content, however the degree of  
628 hydration of the layer is unknown. Nonetheless, the molar peptide loading on GNPs is of similar  
629 order of magnitude to that of the SpyCatcher MNPs. When adsorbing in a monolayer, the molar  
630 surface density of peptides is expected to be higher than the bulkier proteins due to the smaller  
631 size.<sup>65</sup> However, in this case, the comparison is made between monolayer of LanM1 peptide and  
632 lanmodulin protein immobilized on the branched polymer (SpyCatcher) functionalized on MNPs.  
633 The branched polymer provides a three-dimensional scaffold onto which the proteins can be  
634 conjugated whereas the peptides were directly conjugated to the gold nanoparticle surface in a  
635 monolayer. The three-dimensional structure of the brushes provides additional capacity per unit  
636 surface area of the underlying MNP. In addition, the lanmodulin protein has more available REE  
637 binding sites per mole than the LanM1 peptide, thus resulting in an appropriately lower saturated  
638 binding capacity for the material in this study. One study had shown that immobilized lanmodulin  
639 protein had two sites available for REE binding in comparison to three in the solution.<sup>22</sup> The study  
640 suggested inaccessibility of one site upon immobilization. We note that our estimated molar  
641 loading of peptide is close the saturated adsorption capacity measured of  $\sim 3.5$   $\mu\text{mol}$  of REE per g  
642 of GNP-LanM1, indicating high site accessibility. Lanmodulin protein has a molecular weight  
643 that is  $\sim 7$  times higher than the LanM1 peptide, indicating that the maximum adsorption capacity  
644 achieved with the peptide is relatively high when considering the mass of peptide used compared  
645 to the lanmodulin-MNP material. While this comparison is useful, we note it is difficult to compare  
646 the two studies because adsorption capacity can depend on several factors.<sup>66</sup>

### 647 3 Conclusion

648 In summary, LanM1 peptide derived from the EF-hand loop 1 of lanmodulin was tested for its  
649 binding affinity for different REEs, Ce (III), Nd (III), Eu (III) and Y (III), both in bulk and when  
650 bound to a gold surface using both experimental and computational techniques. The ability of Ce  
651 (III) ions to bind with LanM1 and scrambled LanM1 was confirmed using circular dichroism (CD)  
652 and corroborated using molecular dynamics and nuclear magnetic resonance spectroscopy (NMR)  
653 analysis. Isothermal titration calorimetry (ITC) results showed spontaneous binding for all REEs  
654 to the LanM1 peptide. The binding was enthalpically disfavored but driven by a positive change  
655 in entropy. The dissociation constants from ITC were correlated to the ionic radius of REEs with  
656 a  $K_d$  of  $3.84 \pm 1.47$ ,  $1.44 \pm 0.07$  and  $0.80 \pm 0.48 \mu\text{M}$  for Ce (III), Nd (III) and Eu (III), respectively.  
657 In the case of non-REE ions, calcium Ca (II) and Cu (II), no affinity with LanM1 was observed.  
658 At pH below 2, Ce (III) was not observed to bind with LanM1, suggesting pH swing as a possible  
659 regeneration mechanism. Quartz crystal microbalance with dissipation (QCM-D) analysis was  
660 performed to characterize the binding of REEs and non-REEs to surface-immobilized LanM1. The  
661 dissociation constants obtained from Langmuir model fitting suggested that the binding affinities  
662 for Ce (III) and Nd (III) with surface bound LanM1 were estimated to be roughly  $\sim 0.9$  and  $1.8$   
663  $\mu\text{M}$ , respectively. The saturated adsorption capacity of LanM1 immobilized on gold nanoparticles  
664 were estimated using arsenazo-III based colorimetric dye-displacement assay and UV-vis  
665 spectrophotometry to be around  $3.5 \mu\text{mol}$  of REE/mg of GNP-LanM1, with negligible binding to  
666 Ca (II) ions. Overall, this study demonstrates the potential for surface-bound LanM1 peptides to  
667 have high affinity for REEs and be used in advanced separation technologies. The work also  
668 motivates future studies to investigate how immobilizing this peptide might impact trends in REE

669 affinity and how the LanM1 peptide sequence might be manipulated to optimize the separation of  
670 REE mixtures.

## 671 **Acknowledgements**

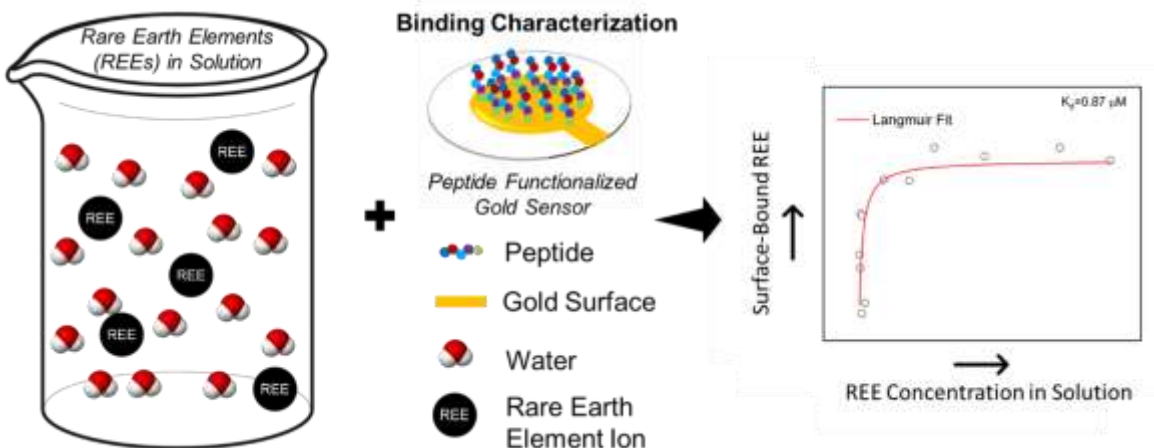
672 We acknowledge Molecular Biotechnology Core at Cleveland Clinic and thank Dr. Smarajit  
673 Bandyopadhyay, Director, Molecular Biotechnology Core for his help with CD and ITC  
674 experiments. A special thanks to Sayani Biswas, a graduate student in the Department of Chemical  
675 and Biomolecular Engineering at Ohio State University for validating MD calculations. We also  
676 thank Dr. Jeffrey Capadona, professor in the Department of Biomedical Engineering at Case  
677 Western Reserve University for allowing us to use QCM-D instrument in his lab. This work used  
678 the Extreme Science and Engineering Discovery Environment (XSEDE), which is supported by  
679 National Science Foundation grant number ACI-1548562. Specifically, it used the Bridges-2  
680 system, which is supported by NSF award number ACI-1928147, at the Pittsburgh  
681 Supercomputing Center (PSC). The project is supported by the National Science Foundation ECO-  
682 CBET program, award #2133549. We also acknowledge the use of instruments at the NMR center  
683 at the Georgia Institute of Technology.

## 684 **Supporting Information**

685 Additional experimental results and data, including a snapshot of molecular dynamics system;  
686 NMR results, ITC results; QCM-D results; Scatchard plot; Langmuir model regression data,  
687 Summary of adsorption metrics used in the selectivity analysis; Estimated adsorption capacities  
688 for REEs using GNPs; Derivation for a two-step Scatchard analysis. A repository of the  
689 GROMCAS input files is created on GitHub: [https://github.com/gev28/Gromacs\\_input\\_file](https://github.com/gev28/Gromacs_input_file).

## 690 **Table Of Contents (TOC) graphic**

691



692

693

## 694 References

- 695 1. Hossain, M. K.; Raihan, G. A.; Akbar, M. A.; Kabir Rubel, M. H.; Ahmed, M. H.; Khan, M. I.;  
696 Hossain, S.; Sen, S. K.; Jalal, M. I. E.; El-Denglawey, A., Current Applications and Future Potential of Rare  
697 Earth Oxides in Sustainable Nuclear, Radiation, and Energy Devices: A Review. *ACS Applied Electronic*  
698 *Materials* **2022**, 4 (7), 3327-3353.
- 699 2. Elbashier, E.; Mussa, A.; Hafiz, M.; Hawari, A. H., Recovery of rare earth elements from waste  
700 streams using membrane processes: An overview. *Hydrometallurgy* **2021**, 204, 105706.
- 701 3. Ni'am, A. C.; Wang, Y.-F.; Chen, S.-W.; Chang, G.-M.; You, S.-J., Simultaneous recovery of rare  
702 earth elements from waste permanent magnets (WPMs) leach liquor by solvent extraction and hollow  
703 fiber supported liquid membrane. *Chemical Engineering and Processing - Process Intensification* **2020**,  
704 148, 107831.
- 705 4. Murthy, Z.; Choudhary, A., Separation of cerium from feed solution by nanofiltration.  
706 *Desalination* **2011**, 279 (1-3), 428-432.
- 707 5. Fritz, J. S., Early milestones in the development of ion-exchange chromatography: a personal  
708 account. *Journal of Chromatography A* **2004**, 1039 (1), 3-12.
- 709 6. Hassas, B. V.; Rezaee, M.; Pisupati, S. V., Effect of various ligands on the selective precipitation  
710 of critical and rare earth elements from acid mine drainage. *Chemosphere* **2021**, 280, 130684.
- 711 7. Park, D.; Middleton, A.; Smith, R.; Deblonde, G.; Laudal, D.; Theaker, N.; Hsu-Kim, H.; Jiao, Y.,  
712 A biosorption-based approach for selective extraction of rare earth elements from coal byproducts.  
713 *Separation and Purification Technology* **2020**, 241, 116726.
- 714 8. Castrillejo, Y.; Bermejo, M. R.; Pardo, R.; Martínez, A. M., Use of electrochemical techniques for  
715 the study of solubilization processes of cerium-oxide compounds and recovery of the metal from  
716 molten chlorides. *Journal of Electroanalytical Chemistry* **2002**, 522 (2), 124-140.
- 717 9. Mwewa, B.; Tadie, M.; Ndlovu, S.; Simate, G. S.; Matinde, E., Recovery of rare earth elements  
718 from acid mine drainage: A review of the extraction methods. *Journal of Environmental Chemical*  
719 *Engineering* **2022**, 10 (3), 107704.

- 720 10. Chen, Z.; Li, Z.; Chen, J.; Kallem, P.; Banat, F.; Qiu, H., Recent advances in selective separation  
721 technologies of rare earth elements: a review. *Journal of Environmental Chemical Engineering* **2022**, *10*  
722 (1), 107104.
- 723 11. Bashiri, A.; Nikzad, A.; Maleki, R.; Asadnia, M.; Razmjou, A., Rare Earth Elements Recovery  
724 Using Selective Membranes via Extraction and Rejection. *Membranes* **2022**, *12* (1), 80.
- 725 12. Ambaye, T. G.; Vaccari, M.; Castro, F. D.; Prasad, S.; Rtimi, S., Emerging technologies for the  
726 recovery of rare earth elements (REEs) from the end-of-life electronic wastes: a review on progress,  
727 challenges, and perspectives. *Environmental Science and Pollution Research* **2020**, *27* (29), 36052-36074.
- 728 13. Braun, R.; Bachmann, S.; Schönberger, N.; Matys, S.; Lederer, F.; Pollmann, K., Peptides as  
729 biosorbents – Promising tools for resource recovery. *Research in Microbiology* **2018**, *169* (10), 649-658.
- 730 14. Wallin, C.; Kulkarni, Y. S.; Abelein, A.; Jarvet, J.; Liao, Q.; Strodel, B.; Olsson, L.; Luo, J.;  
731 Abrahams, J. P.; Sholts, S. B.; Roos, P. M.; Kamerlin, S. C. L.; Gräslund, A.; Wärmländer, S. K. T. S.,  
732 Characterization of Mn(II) ion binding to the amyloid- $\beta$  peptide in Alzheimers disease. *Journal of Trace*  
733 *Elements in Medicine and Biology* **2016**, *38*, 183-193.
- 734 15. Hatanaka, T.; Kikkawa, N.; Matsugami, A.; Hosokawa, Y.; Hayashi, F.; Ishida, N., The origins of  
735 binding specificity of a lanthanide ion binding peptide. *Scientific Reports* **2020**, *10* (1), 19468.
- 736 16. Xu, M.; Su, Z.; Renner, J. N., Characterization of cerium (III) ion binding to surface-immobilized  
737 EF-hand loop I of calmodulin. *Peptide Science* **2019**, *111* (6), e24133.
- 738 17. Su, Z.; Hostert, J. D.; Renner, J. N., Phosphate Recovery by a Surface-Immobilized Cerium  
739 Affinity Peptide. *ACS ES&T Water* **2021**, *1* (1), 58-67.
- 740 18. Cotruvo, J. A., Jr.; Featherston, E. R.; Mattocks, J. A.; Ho, J. V.; Laremore, T. N., Lanmodulin: A  
741 Highly Selective Lanthanide-Binding Protein from a Lanthanide-Utilizing Bacterium. *Journal of the*  
742 *American Chemical Society* **2018**, *140* (44), 15056-15061.
- 743 19. Deblonde, G. J. P.; Mattocks, J. A.; Park, D. M.; Reed, D. W.; Cotruvo, J. A.; Jiao, Y., Selective  
744 and Efficient Biomacromolecular Extraction of Rare-Earth Elements using Lanmodulin. *Inorganic*  
745 *Chemistry* **2020**, *59* (17), 11855-11867.
- 746 20. Xie, X.; Yang, K.; Lu, Y.; Li, Y.; Yan, J.; Huang, J.; Xu, L.; Yang, M.; Yan, Y., Broad-spectrum and  
747 effective rare earth enriching via Lanmodulin-displayed *Yarrowia lipolytica*. *Journal of Hazardous*  
748 *Materials* **2022**, *438*, 129561.
- 749 21. Hussain, Z.; Kim, S.; Cho, J.; Sim, G.; Park, Y.; Kwon, I., Repeated Recovery of Rare Earth  
750 Elements Using a Highly Selective and Thermo-Responsive Genetically Encoded Polypeptide. *Advanced*  
751 *Functional Materials* **2022**, *32* (13), 2109158.
- 752 22. Dong, Z.; Mattocks, J. A.; Deblonde, G. J. P.; Hu, D.; Jiao, Y.; Cotruvo, J. A., Jr.; Park, D. M.,  
753 Bridging Hydrometallurgy and Biochemistry: A Protein-Based Process for Recovery and Separation of  
754 Rare Earth Elements. *ACS Central Science* **2021**, *7* (11), 1798-1808.
- 755 23. Ye, Q.; Jin, X.; Zhu, B.; Gao, H.; Wei, N., Lanmodulin-Functionalized Magnetic Nanoparticles as  
756 a Highly Selective Biosorbent for Recovery of Rare Earth Elements. *Environmental Science & Technology*  
757 **2023**, *57* (10), 4276-4285.
- 758 24. Gutenthaler, S.; Tsushima, S.; Steudtner, R.; Gailer, M.; Hoffmann-Röder, A.; Drobot, B.;  
759 Daumann, L., LanM Peptides–Unravelling the Binding Properties of the EF-Hand Loop Sequences  
760 Stripped from the Structural Corset. *Inorganic Chemistry Frontiers* **2021**, *9* (16), 4009-4021.
- 761 25. Gerblinger, J.; Lohwasser, W.; Lampe, U.; Meixner, H., High temperature oxygen sensor based  
762 on sputtered cerium oxide. *Sensors and Actuators B: Chemical* **1995**, *26* (1), 93-96.
- 763 26. El Idrissi, B.; Addou, M.; Outzourhit, A.; Regragui, M.; Bougrine, A.; Kachouane, A., Sprayed  
764 CeO<sub>2</sub> thin films for electrochromic applications. *Solar Energy Materials and Solar Cells* **2001**, *69* (1), 1-8.
- 765 27. Charalampides, G.; Vatalis, K. I.; Apostoplos, B.; Ploutarch-Nikolas, B., Rare Earth Elements:  
766 Industrial Applications and Economic Dependency of Europe. *Procedia Economics and Finance* **2015**, *24*,  
767 126-135.

768 28. Patil, A. S.; Patil, A. V.; Dighavkar, C. G.; Adole, V. A.; Tupe, U. J., Synthesis techniques and  
769 applications of rare earth metal oxides semiconductors: A review. *Chemical Physics Letters* **2022**, *796*,  
770 139555.

771 29. Hossain, M. K.; Hossain, S.; Ahmed, M. H.; Khan, M. I.; Haque, N.; Raihan, G. A., A Review on  
772 Optical Applications, Prospects, and Challenges of Rare-Earth Oxides. *ACS Applied Electronic Materials*  
773 **2021**, *3* (9), 3715-3746.

774 30. Humphrey, W.; Dalke, A.; Schulten, K., VMD: Visual molecular dynamics. *Journal of Molecular*  
775 *Graphics* **1996**, *14* (1), 33-38.

776 31. Su, Z. H.; Pramounmat, N.; Watson, S. T.; Renner, J. N., Engineered interaction between short  
777 elastin-like peptides and perfluorinated sulfonic-acid ionomer. *Soft Matter* **2018**, *14* (18), 3528-3535.

778 32. Van Der Spoel, D.; Lindahl, E.; Hess, B.; Groenhof, G.; Mark, A. E.; Berendsen, H. J. C.,  
779 GROMACS: Fast, flexible, and free. *Journal of Computational Chemistry* **2005**, *26* (16), 1701-1718.

780 33. Goddard, T. D.; Huang, C. C.; Meng, E. C.; Pettersen, E. F.; Couch, G. S.; Morris, J. H.; Ferrin, T.  
781 E., UCSF ChimeraX: Meeting modern challenges in visualization and analysis. *Protein Sci* **2018**, *27* (1), 14-  
782 25.

783 34. Brooks, B. R.; Bruccoleri, R. E.; Olafson, B. D.; States, D. J.; Swaminathan, S.; Karplus, M.,  
784 CHARMM: A program for macromolecular energy, minimization, and dynamics calculations. *Journal of*  
785 *Computational Chemistry* **1983**, *4* (2), 187-217.

786 35. Sinitsyn, A. V.; Gracheva, M. E., Atomistic model of a ceria nanoparticle with Ce(3 + ) and Ce(4 + )  
787 atoms. *Nanotechnology* **2020**, *31* (31), 315708.

788 36. Migliorati, V.; Serva, A.; Terenzio, F. M.; D'Angelo, P., Development of Lennard-Jones and  
789 Buckingham Potentials for Lanthanoid Ions in Water. *Inorganic Chemistry* **2017**, *56* (11), 6214-6224.

790 37. Li, P.; Song, L. F.; Merz, K. M., Jr., Parameterization of Highly Charged Metal Ions Using the 12-6-  
791 4 LJ-Type Nonbonded Model in Explicit Water. *The Journal of Physical Chemistry B* **2015**, *119* (3), 883-  
792 895.

793 38. Duan, L.; Liu, X.; Zhang, J. Z. H., Interaction Entropy: A New Paradigm for Highly Efficient and  
794 Reliable Computation of Protein-Ligand Binding Free Energy. *Journal of the American Chemical Society*  
795 **2016**, *138* (17), 5722-5728.

796 39. Hess, B.; Kutzner, C.; van der Spoel, D.; Lindahl, E., GROMACS 4: Algorithms for Highly Efficient,  
797 Load-Balanced, and Scalable Molecular Simulation. *Journal of Chemical Theory and Computation* **2008**, *4*  
798 (3), 435-447.

799 40. Darden, T.; York, D.; Pedersen, L., Particle mesh Ewald: An N·log(N) method for Ewald sums in  
800 large systems. *The Journal of Chemical Physics* **1993**, *98* (12), 10089-10092.

801 41. Bussi, G.; Donadio, D.; Parrinello, M., Canonical sampling through velocity rescaling. *The Journal*  
802 *of Chemical Physics* **2007**, *126* (1), 014101.

803 42. Parrinello, M.; Rahman, A., Polymorphic transitions in single crystals: A new molecular dynamics  
804 method. *Journal of Applied Physics* **1981**, *52* (12), 7182-7190.

805 43. Cook, E. C.; Featherston, E. R.; Showalter, S. A.; Cotruvo, J. A., Structural Basis for Rare Earth  
806 Element Recognition by Methylobacterium extorquens Lanmodulin. *Biochemistry* **2019**, *58* (2), 120-125.

807 44. Habenschuss, A.; Spedding, F. H., The coordination (hydration) of rare earth ions in aqueous  
808 chloride solutions from x-ray diffraction. III. SmCl<sub>3</sub>, EuCl<sub>3</sub>, and series behavior. *The Journal of Chemical*  
809 *Physics* **2008**, *73* (1), 442-450.

810 45. Liu, S.; Featherston, E. R.; Cotruvo, J. A.; Baiz, C. R., Lanthanide-dependent coordination  
811 interactions in lanmodulin: a 2D IR and molecular dynamics simulations study. *Physical Chemistry*  
812 *Chemical Physics* **2021**, *23* (38), 21690-21700.

813 46. Hoch, J. C.; Baskaran, K.; Burr, H.; Chin, J.; Eghbalnia, H. R.; Fujiwara, T.; Gryk, M. R.; Iwata,  
814 T.; Kojima, C.; Kurisu, G., Biological magnetic resonance data bank. *Nucleic acids research* **2023**, *51* (D1),  
815 D368-D376.

- 816 47. Clore, G. M., Chapter Seventeen - Practical Aspects of Paramagnetic Relaxation Enhancement in  
817 Biological Macromolecules. In *Methods in Enzymology*, Qin, P. Z.; Warncke, K., Eds. Academic Press:  
818 2015; Vol. 564, pp 485-497.
- 819 48. Karschin, N.; Becker, S.; Griesinger, C., Interdomain Dynamics via Paramagnetic NMR on the  
820 Highly Flexible Complex Calmodulin/Munc13-1. *Journal of the American Chemical Society* **2022**, *144* (37),  
821 17041-17053.
- 822 49. Müntener, T.; Joss, D.; Häussinger, D.; Hiller, S., Pseudocontact shifts in biomolecular NMR  
823 spectroscopy. *Chemical Reviews* **2022**, *122* (10), 9422-9467.
- 824 50. Bahramzadeh, A.; Huber, T.; Otting, G., Three-Dimensional Protein Structure Determination  
825 Using Pseudocontact Shifts of Backbone Amide Protons Generated by Double-Histidine Co<sup>2+</sup>-Binding  
826 Motifs at Multiple Sites. *Biochemistry* **2019**, *58* (30), 3243-3250.
- 827 51. Lopez, M. M.; Chin, D. H.; Baldwin, R. L.; Makhatadze, G. I., The enthalpy of the alanine peptide  
828 helix measured by isothermal titration calorimetry using metal-binding to induce helix formation. *Proc*  
829 *Natl Acad Sci U S A* **2002**, *99* (3), 1298-302.
- 830 52. Nitz, M.; Sherawat, M.; Franz, K. J.; Peisach, E.; Allen, K. N.; Imperiali, B., Structural Origin of  
831 the High Affinity of a Chemically Evolved Lanthanide-Binding Peptide. *Angewandte Chemie International*  
832 *Edition* **2004**, *43* (28), 3682-3685.
- 833 53. Snyder, E. E.; Buoscio, B. W.; Falke, J. J., Calcium(II) site specificity: effect of size and charge on  
834 metal ion binding to an EF-hand-like site. *Biochemistry* **1990**, *29* (16), 3937-3943.
- 835 54. Stewart, B. W.; Capo, R. C.; Hedin, B. C.; Hedin, R. S., Rare earth element resources in coal mine  
836 drainage and treatment precipitates in the Appalachian Basin, USA. *International Journal of Coal*  
837 *Geology* **2017**, *169*, 28-39.
- 838 55. Easley, A. D.; Ma, T.; Eneh, C. I.; Yun, J.; Thakur, R. M.; Lutkenhaus, J. L., A practical guide to  
839 quartz crystal microbalance with dissipation monitoring of thin polymer films. *Journal of Polymer Science*  
840 **2022**, *60* (7), 1090-1107.
- 841 56. Zhang, Y.; Du, B.; Chen, X.; Ma, H., Convergence of Dissipation and Impedance Analysis of  
842 Quartz Crystal Microbalance Studies. *Analytical Chemistry* **2009**, *81* (2), 642-648.
- 843 57. Wu, B.; Wan, J.; Zhang, Y.; Pan, B.; Lo, I. M. C., Selective Phosphate Removal from Water and  
844 Wastewater using Sorption: Process Fundamentals and Removal Mechanisms. *Environmental Science &*  
845 *Technology* **2020**, *54* (1), 50-66.
- 846 58. Zhao, F.; Cong, Z.; Sun, H.; Ren, D., The geochemistry of rare earth elements (REE) in acid mine  
847 drainage from the Sitai coal mine, Shanxi Province, North China. *International Journal of Coal Geology*  
848 **2007**, *70* (1), 184-192.
- 849 59. Kalam, S.; Abu-Khamsin, S. A.; Kamal, M. S.; Patil, S., Surfactant Adsorption Isotherms: A  
850 Review. *ACS Omega* **2021**, *6* (48), 32342-32348.
- 851 60. Azizian, S.; Eris, S.; Wilson, L. D., Re-evaluation of the century-old Langmuir isotherm for  
852 modeling adsorption phenomena in solution. *Chemical Physics* **2018**, *513*, 99-104.
- 853 61. Bertelsen, E. R.; Jackson, J. A.; Shafer, J. C., A Survey of Extraction Chromatographic f-Element  
854 Separations Developed by E. P. Horwitz. *Solvent Extraction and Ion Exchange* **2020**, *38* (3), 251-289.
- 855 62. Horwitz, E. P.; McAlister, D. R.; Bond, A. H.; Barrans, R. E., Novel Extraction of Chromatographic  
856 Resins Based on Tetraalkyldiglycolamides: Characterization and Potential Applications. *Solvent*  
857 *Extraction and Ion Exchange* **2005**, *23* (3), 319-344.
- 858 63. Piguet, C.; G. Bünzli, J.-C., Mono- and polymetallic lanthanide-containing functional assemblies:  
859 a field between tradition and novelty. *Chemical Society Reviews* **1999**, *28* (6), 347-358.
- 860 64. Roca-Sabio, A.; Mato-Iglesias, M.; Esteban-Gómez, D.; Tóth, É.; Blas, A. d.; Platas-Iglesias, C.;  
861 Rodríguez-Blas, T., Macrocyclic Receptor Exhibiting Unprecedented Selectivity for Light Lanthanides.  
862 *Journal of the American Chemical Society* **2009**, *131* (9), 3331-3341.

863 65. Perera, Y. R.; Xu, J. X.; Amarasekara, D. L.; Hughes, A. C.; Abbood, I.; Fitzkee, N. C.,  
864 Understanding the Adsorption of Peptides and Proteins onto PEGylated Gold Nanoparticles. *Molecules*  
865 **2021**, *26* (19), 5788.

866 66. Kegl, T.; Košak, A.; Lobnik, A.; Novak, Z.; Kralj, A. K.; Ban, I., Adsorption of rare earth metals  
867 from wastewater by nanomaterials: A review. *Journal of Hazardous Materials* **2020**, *386*, 121632.

868